DIFFUSE SCATTERING BEYOND THE BRAGG PEAKS

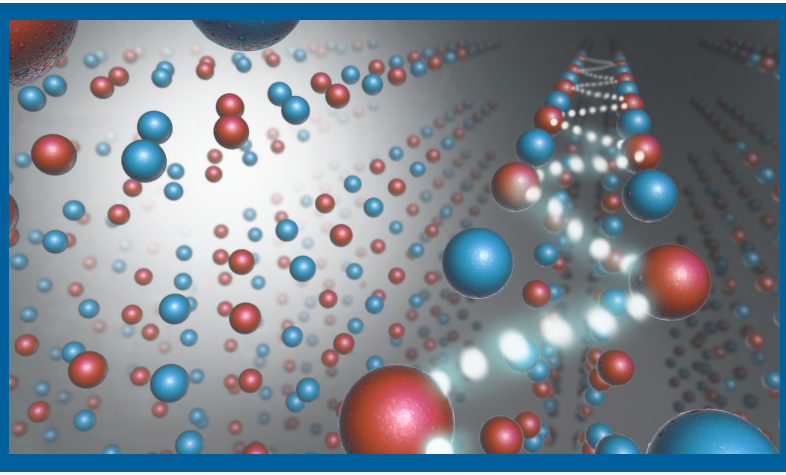

RAYMOND OSBORN
Neutron & X-ray Scattering Group
Materials Science Division

Acknowledgements: Stephan Rosenkranz and Matthew Krogstad

Work supported by the U.S. Department of Energy,
Office of Science, Materials Sciences and Engineering Division.

Neutron & X-ray School
August 17, 2023

OUTLINE

- What is diffuse scattering?
  - What causes it?
- What is it good for?
  - A random walk through disordered materials
- How do I model it?
  - A few equations
- How do I measure it?
- Case Study 1: Diffuse scattering from vacancies in mullite
- Case Study 2: 3D-ΔPDF in sodium-intercalated V_2O_5
- How do I look at static disorder?
  - Diffuse scattering with elastic discrimination

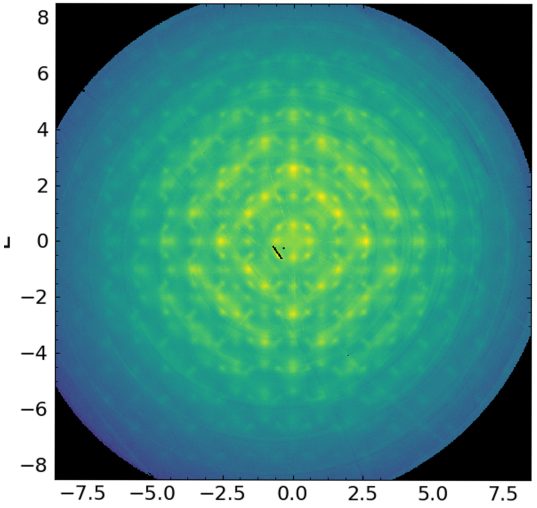

WHAT IS DIFFUSE SCATTERING?

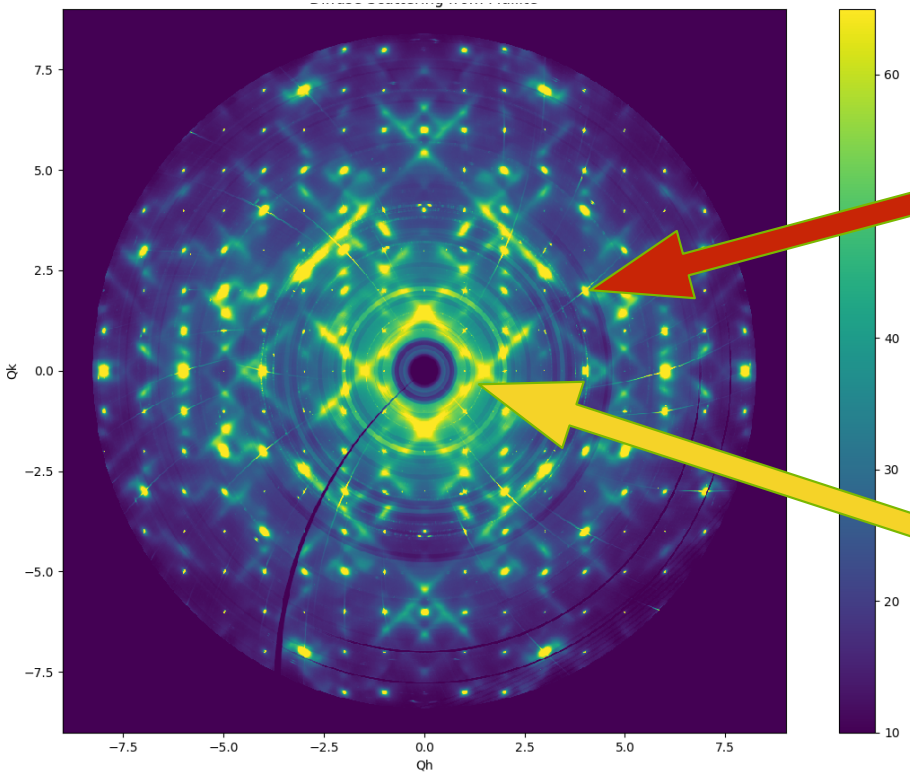

Bragg Scattering
Average Structure

Diffuse Scattering
Deviations from the Average Structure

DIFFUSE SCATTERING

SIMPLE EXAMPLE OF DISORDER

Replace 30% of atoms (blue dots) by vacancies (green dots)

Random Vacancies

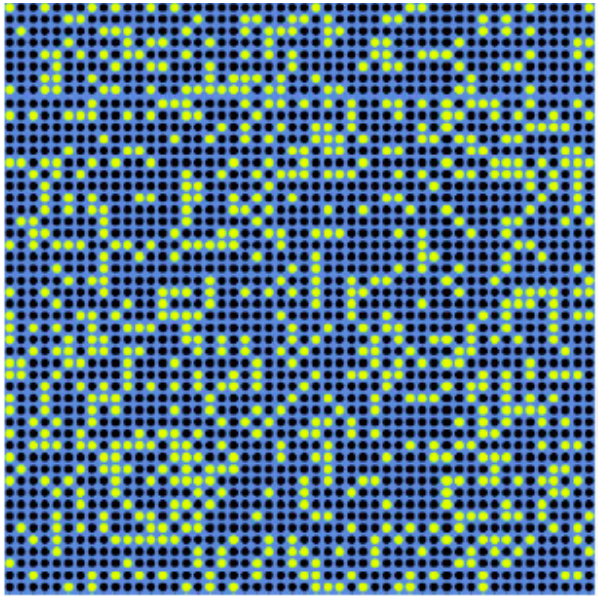

Vacancy Clusters

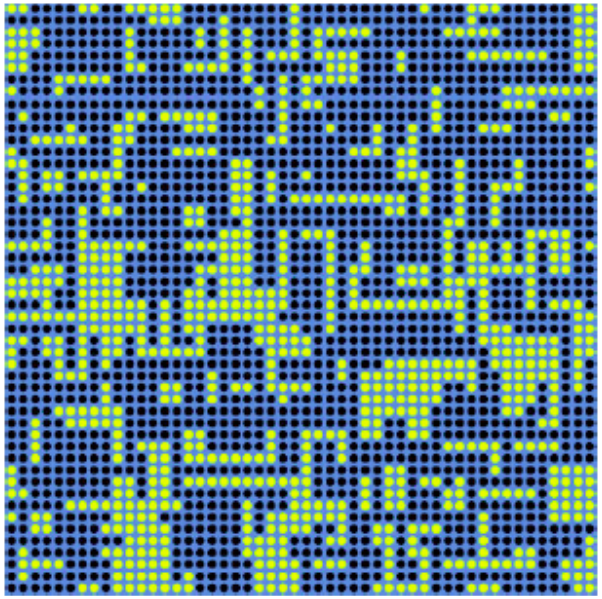

Model due to Thomas Proffen

BRAGG SCATTERING

The average occupancy is unchanged ➡ Bragg peaks are identical

Random Vacancies

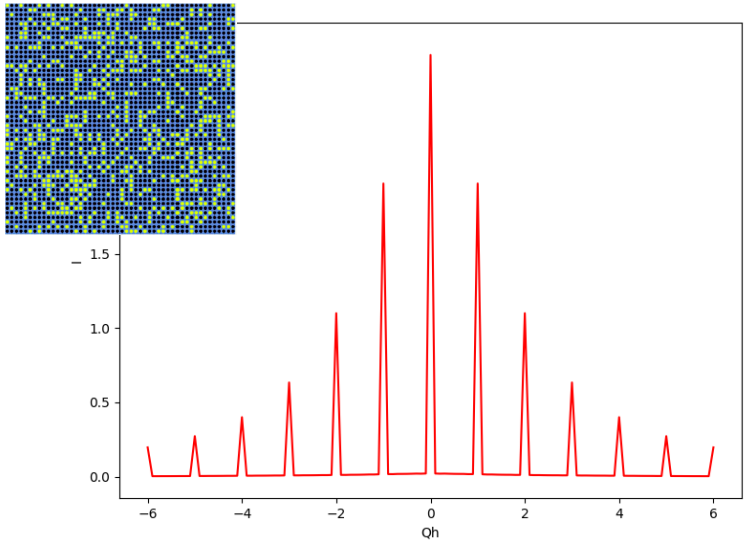

Vacancy Clusters

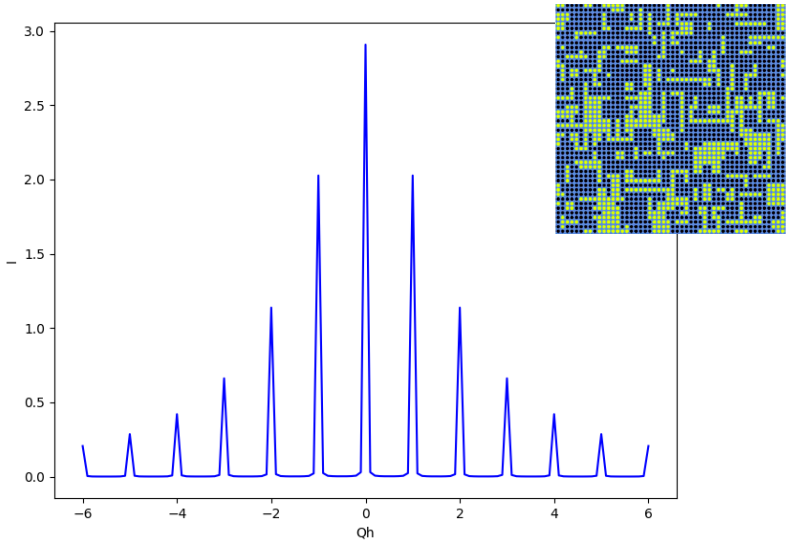

DIFFUSE SCATTERING

The diffuse scattering is quite different.

Random Vacancies

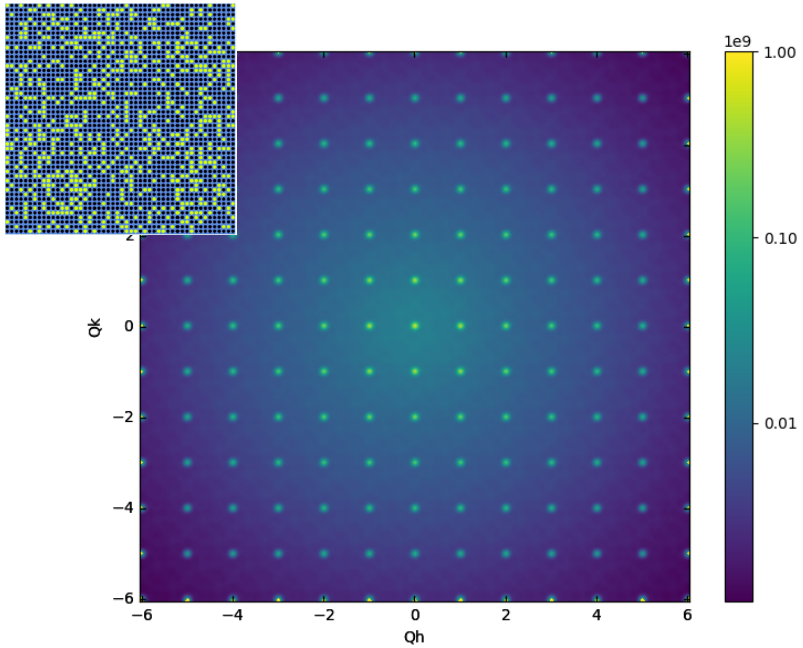

Laue Monotonic Scattering

Vacancy Clusters

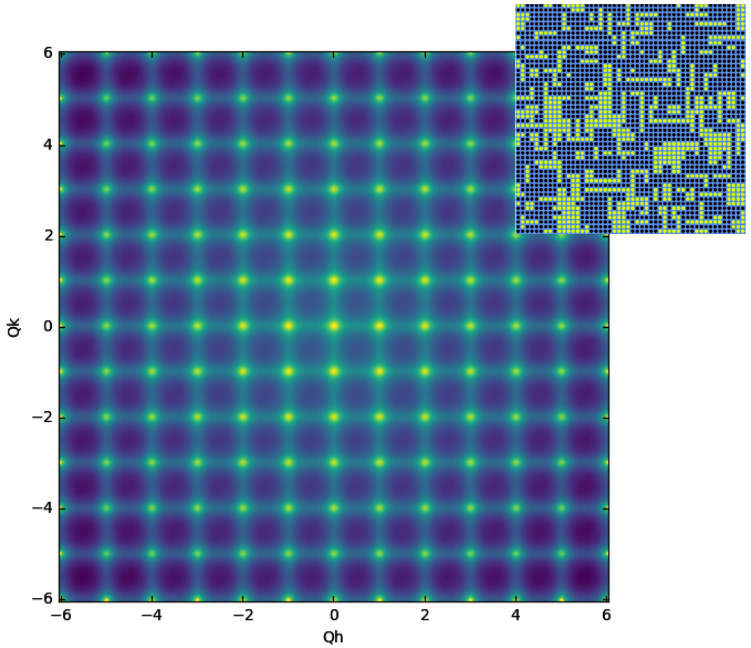

Substitutional Diffuse Scattering

WHAT IS IT GOOD FOR?

DIFFUSE SCATTERING FROM METALLIC ALLOYS

Short-range Order in Null Matrix $^{62}Ni_{0.52}Pt_{0.52}$

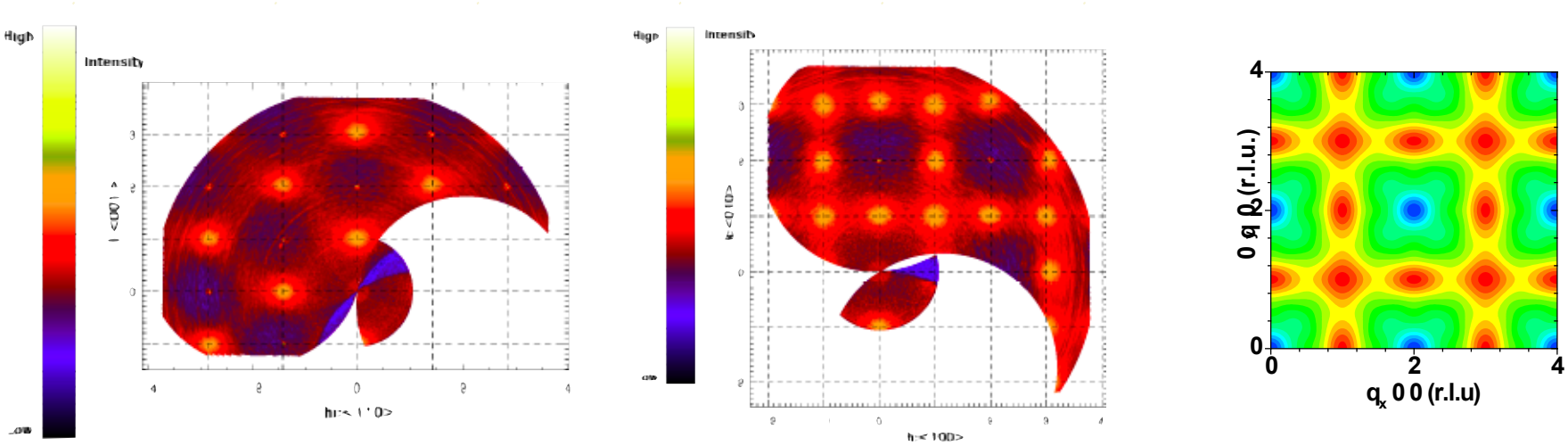

J. A. Rodriguez, *et al*., Phys. Rev. B **74**, 104115

DIFFUSE SCATTERING FROM A FAST-ION CONDUCTOR

Sublattice Melting in Fluorite Compounds

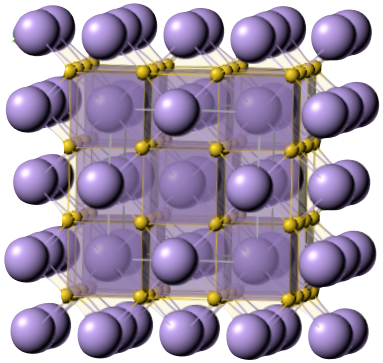

CaF_2

M. T. Hutchings *et al*
J. Phys. C **17**, 3903 (1984)

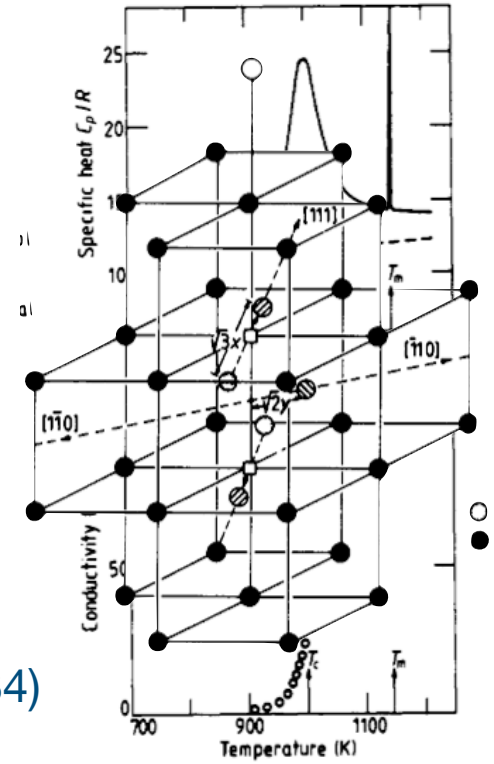

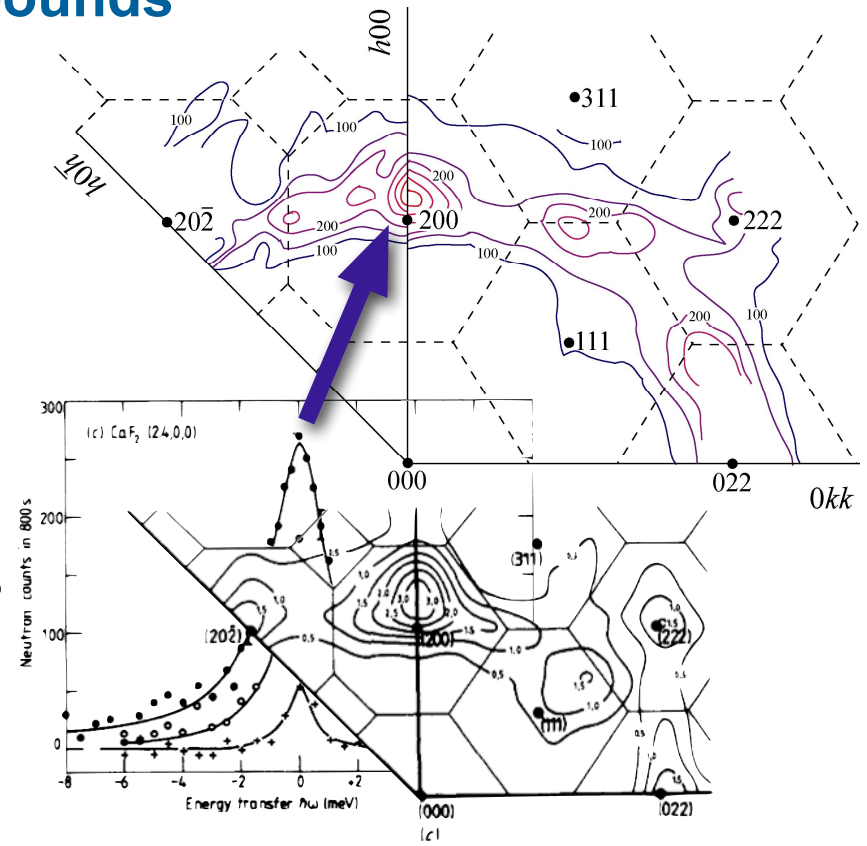

DIFFUSE SCATTERING FROM MOLECULAR SOLIDS

Molecular Flexibility in Benzil

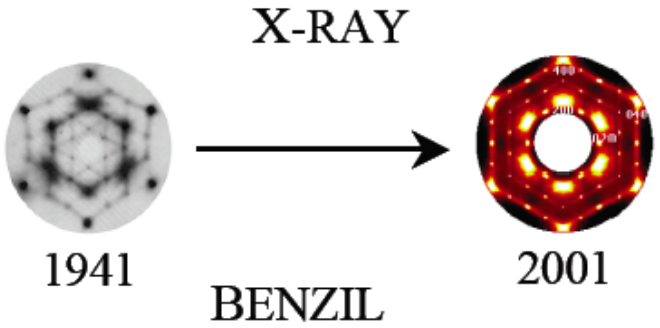

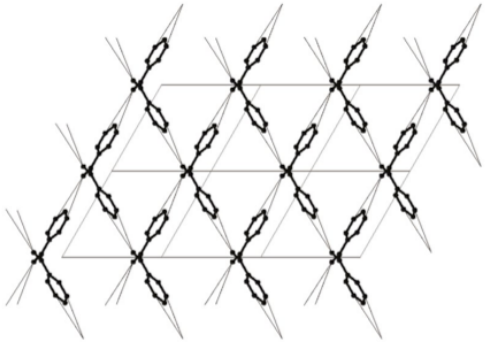

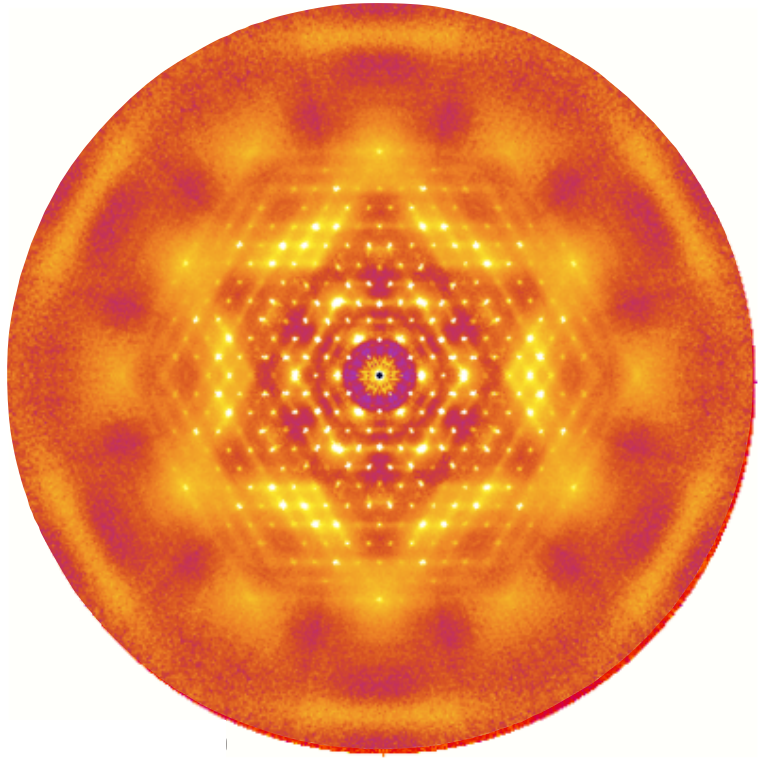

T. R. Welberry *et al* J. Appl. Cryst. **36**, 1400 (2003)

DIFFUSE SCATTERING FROM JAHN-TELLER POLARONS

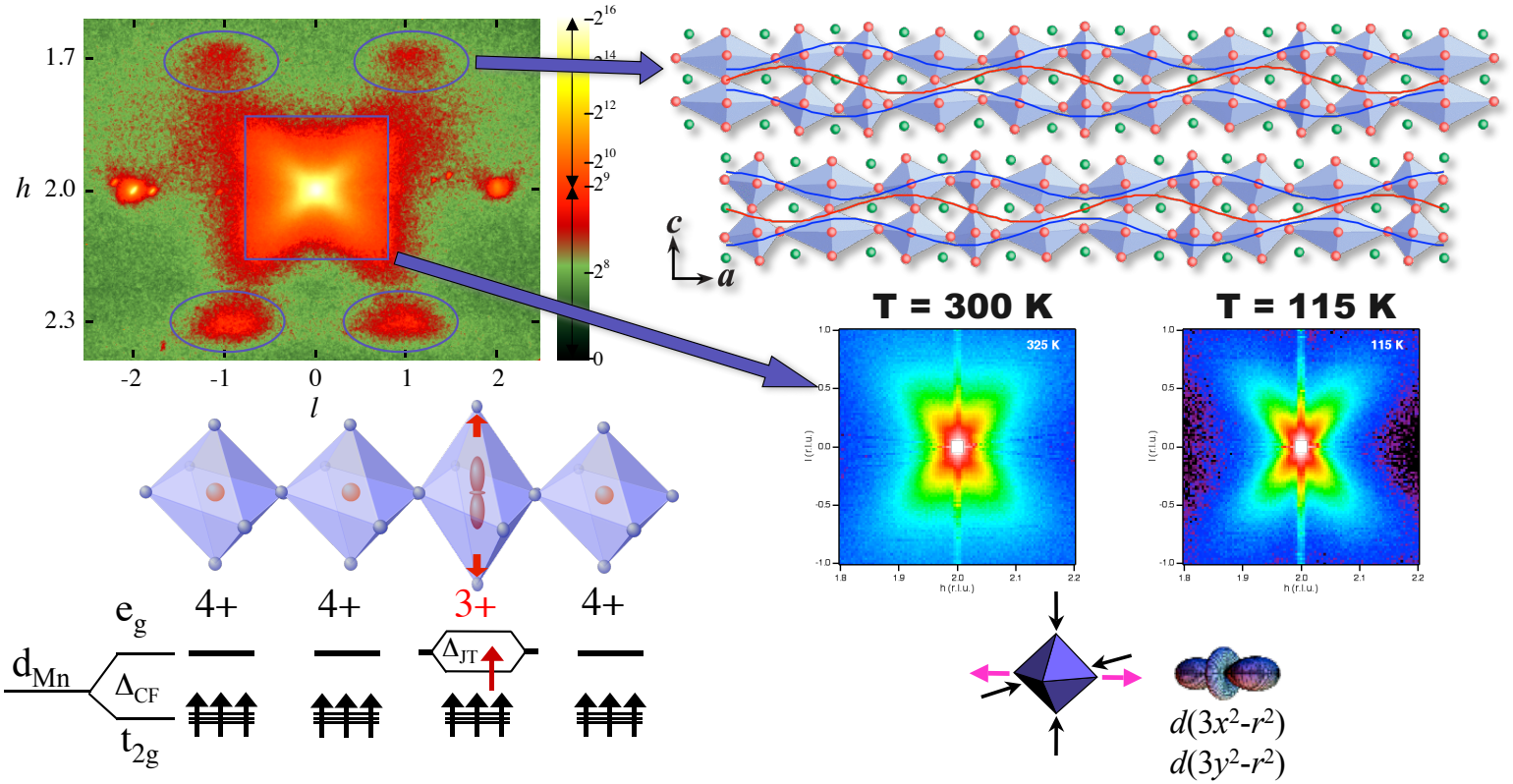

B. J. Campbell, *et al*., Phys Rev B **65**, 014427 (2002).

INCOMMENSURATE MODULATIONS IN $Sr_{0.5}Ba_{0.5}NbO_6$

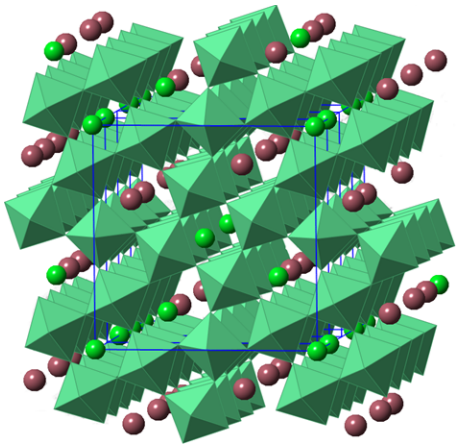

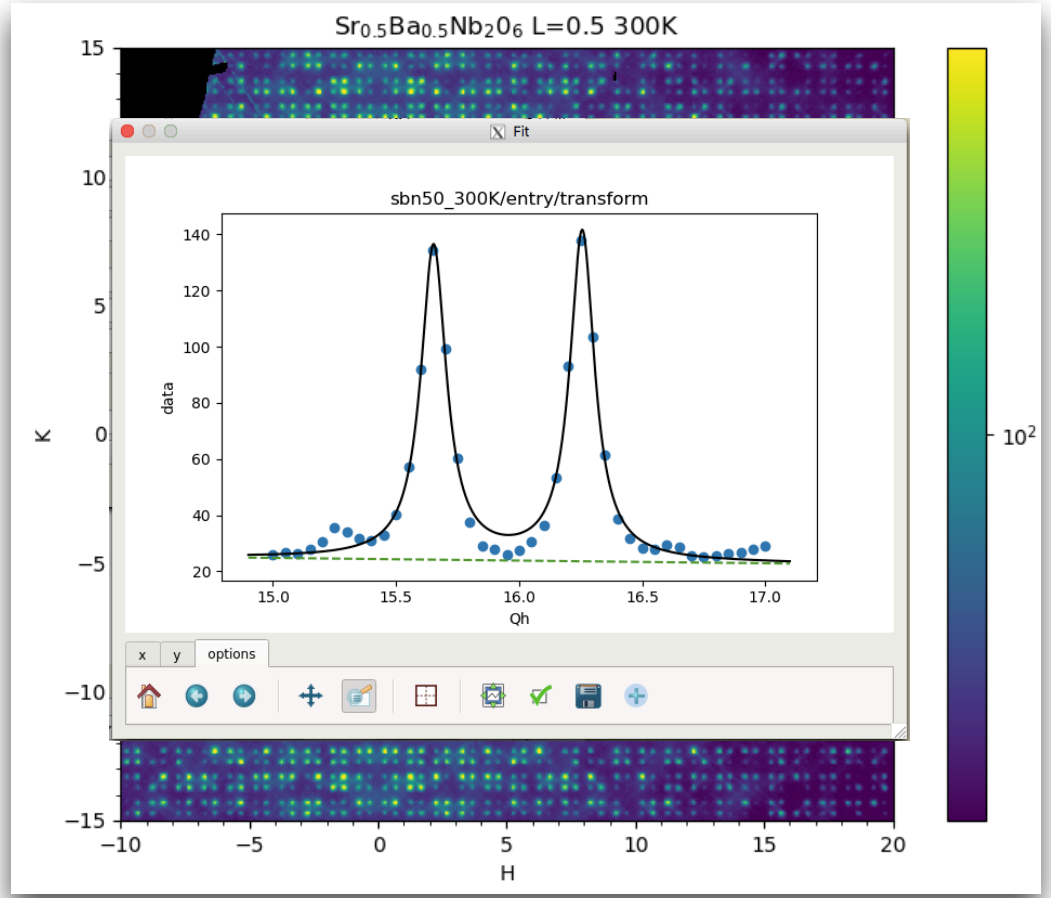

Acknowledgements:
Bixia Wang and Daniel Phelan

MAGNETIC MONOPOLES IN SPIN ICE

Diffuse Magnetic Scattering in $Dy_2Ti_2O_7$

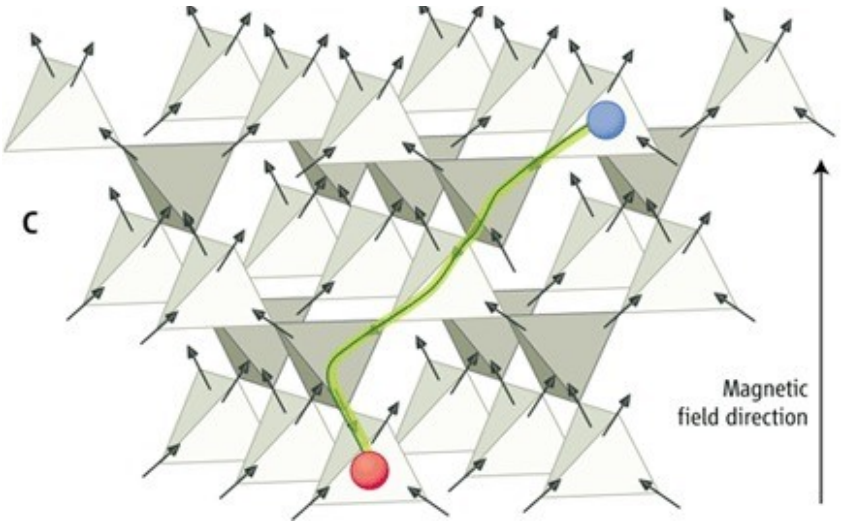

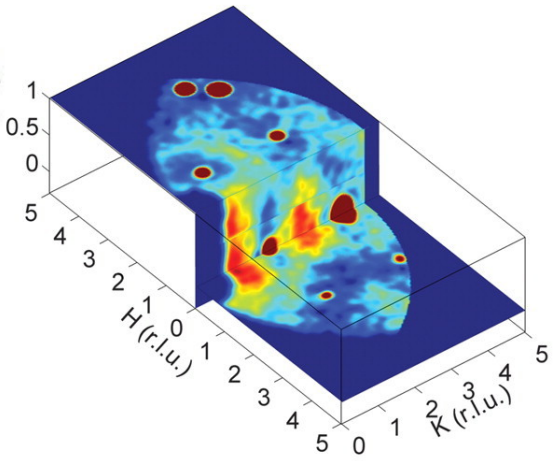

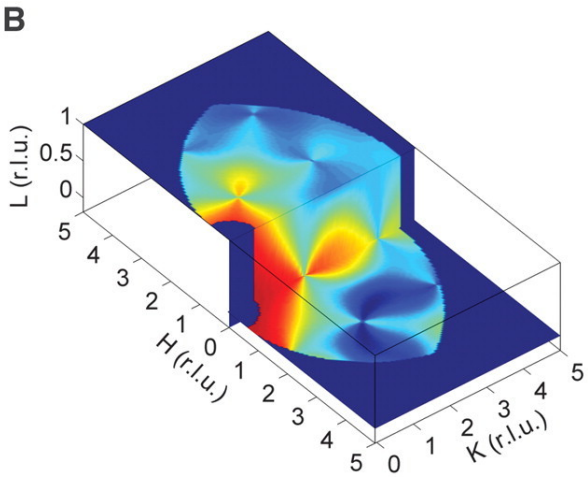

D. J. P. Morris, *et al*., Science **326**, 411 (2009).

HOW DO I MODEL IT?

DIFFUSE SCATTERING THEORY

A Few Equations $I = \sum_i \sum_j b_i b_j \exp(i\mathbf{Q} \cdot \mathbf{r}_{ij})$

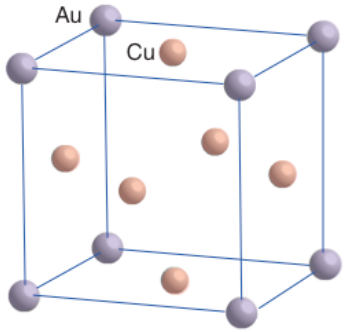

J. M. Cowley, J. Appl. Phys. **21**, 24 (1950)

- **Laue Monotonic Diffuse Scattering**

$$I = \bar{b}^2 \sum_{ij} \exp(i\mathbf{Q} \cdot \mathbf{r}_{ij}) + N(\overline{b^2} - \bar{b}^2);\ \bar{b}^2 = (c_A b_A + c_B b_B)^2;\ \overline{b^2} = c_A c_B (b_B - b_A)^2$$

- **Cowley Short-Range Order**

$$I_{diffuse} = N c_A c_B (b_B - b_A)^2 + \textstyle\sum_{ij} \alpha_{ij} c_B c_A (b_B - b_A)^2 \exp(i\mathbf{Q} \cdot \mathbf{r}_{ij});\ \alpha_{ij} = \left(1 - \frac{P_{ij}}{c_j}\right)$$

- **Warren Size Effect**

$$I_{diffuse} = N c_A c_B (b_B - b_A)^2 \left(1 + \sum_{ij} \alpha_{ij} \exp(i\mathbf{Q} \cdot \mathbf{r}_{ij}) + \beta_{ij} \exp(i\mathbf{Q} \cdot \mathbf{r}_{ij})\right);\ \beta_{ij} = f(\epsilon_{AA}^{ij}, \epsilon_{BB}^{ij})$$

- **Borie and Sparks Correlations**

$$I = \sum_i \sum_j b_i b_j \exp\left(i\mathbf{Q} \cdot (\mathbf{R}_i - \mathbf{R}_j)\right) \left[1 + i\mathbf{Q} \cdot (\mathbf{u}_i - \mathbf{u}_j) - \frac{1}{2} \left(\mathbf{Q} \cdot (\mathbf{u}_i - \mathbf{u}_j)\right)^2 + \ldots\right]$$

V. M. Nield and D. A. Keen *Diffuse Neutron Scattering From Crystalline Materials* (2001)
T. R. Welberry *Diffuse X-ray Scattering and Models of Disorder* (2022)

SOME RULES OF THUMB

Acknowledgment: Hans Beat Bürgi

Reciprocal space

- Sharp Bragg reflections
  - no defects
- Sharp diffuse rods
  - no defects
- Sharp diffuse planes
  - no defects
- Diffuse clouds
  - no defects

Direct space

- 3D-periodic structure
  - no defects
- 2D-periodic structure
  - perpendicular to the streaks
  - disordered in streak directions
- 1D-periodic structure
  - perpendicular to the planes
  - disordered within the plane
- 0D-periodic structure
  - no fully ordered direction

THERMAL DIFFUSE SCATTERING

M. Holt, *et al*, Phys Rev Lett **83**, 3317 (1999).

- Lattice vibrations produce deviations from the average structure even in perfect crystals
- X-ray scattering intensity is given by the integral over all the phonon branches at each Q

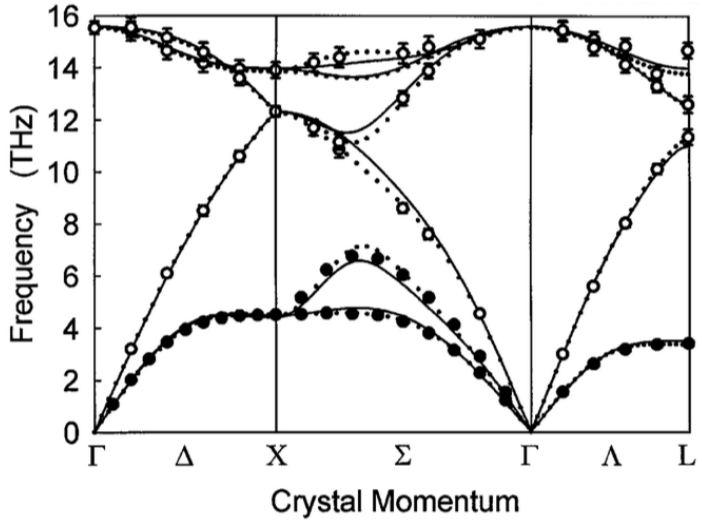

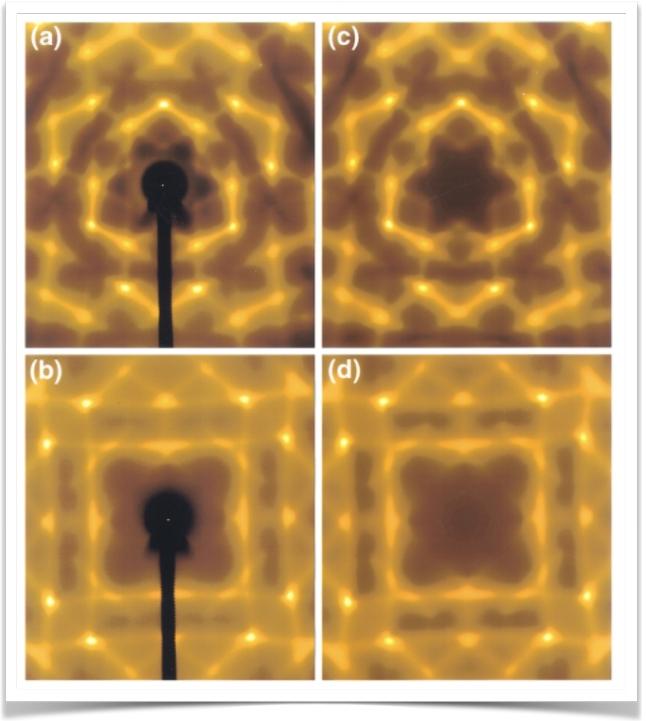

$$I_0 \propto f^2 e^{-2M} \sum_{j=1}^{6} \frac{|\mathbf{q} \cdot \hat{\mathbf{e}}_j|^2}{\omega_j} \coth\left(\frac{\hbar\omega_j}{2k_B T}\right).$$

HOW DO I MEASURE IT?

MEASURING X-RAY DIFFUSE SCATTERING

Continuous Rotation Method

Sector 6 - APS

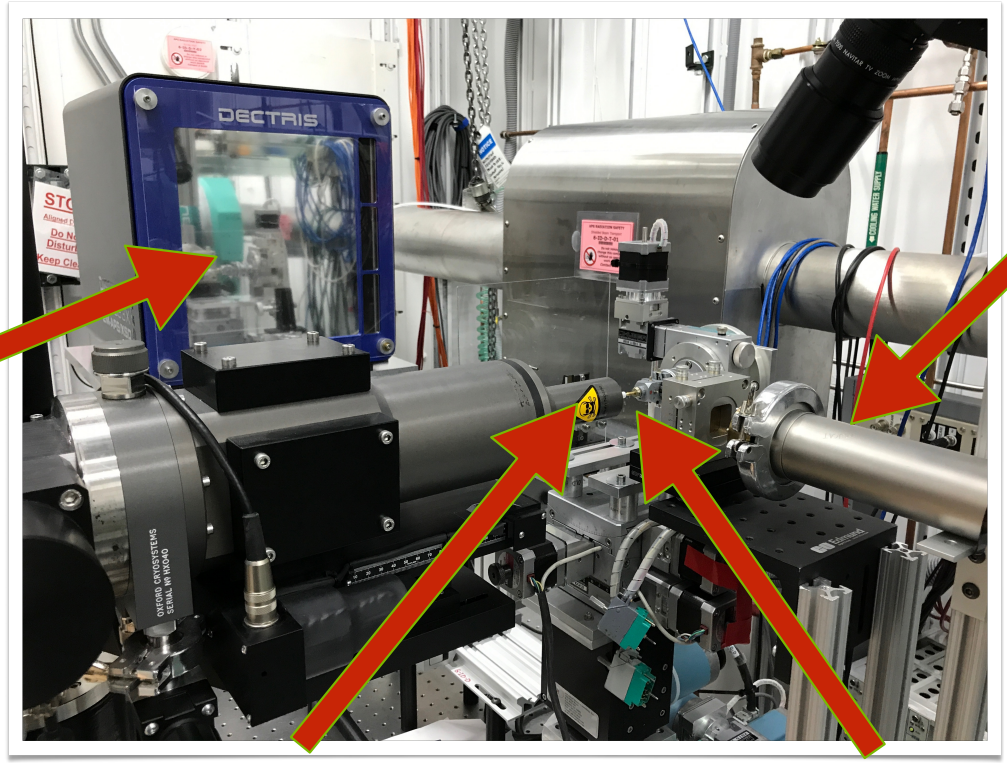

Incident Beam

Detector

Cryocooler

Sample

X-RAY SCATTERING GEOMETRY

Continuous Rotation Method

- The sample is continuously rotated at 1°s^{-1}
- Frames are collected at 10Hz
  - 3600 x 8MB frames
  - 30GB every 6 minutes
  - 3TB per day

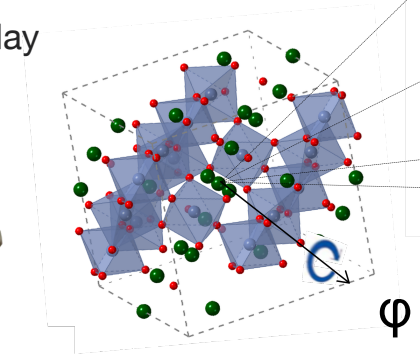

Incident Beam

Sample

Pilatus 2M CdTe Detector

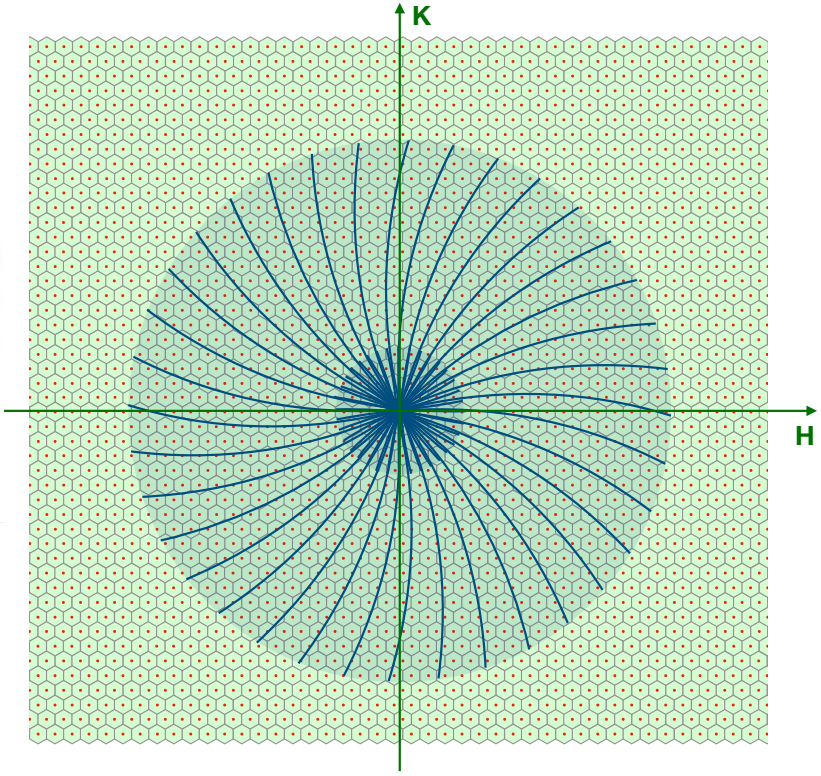

Reciprocal Space

Q-RANGE IN ROTATION METHOD ON SECTOR 6

- With the following parameters, we cover $-15Å^{-1}<\mathbf{Q}<15Å^{-1}$
  - E_i ~ 87 keV
  - λ ~ 0.14 Å
  - Detector distance ~650 mm
  - Pilatus 2M CdTe: 1679x1475 pixels
  - Pixel size ~170 μm
- This Q-range includes thousands of Brillouin zones.
  - *e.g.*, for *a* ~ 10 Å, ~60,000 Bragg peaks

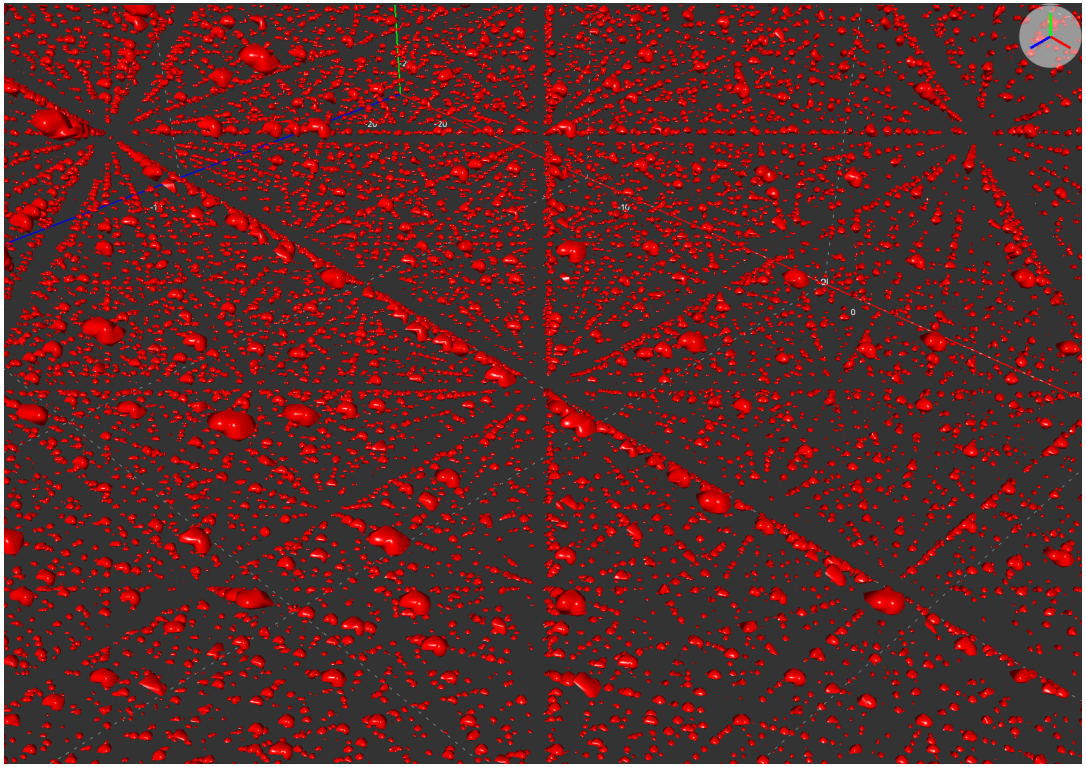

EXPERIMENT WORKFLOW

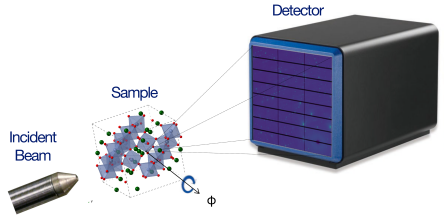

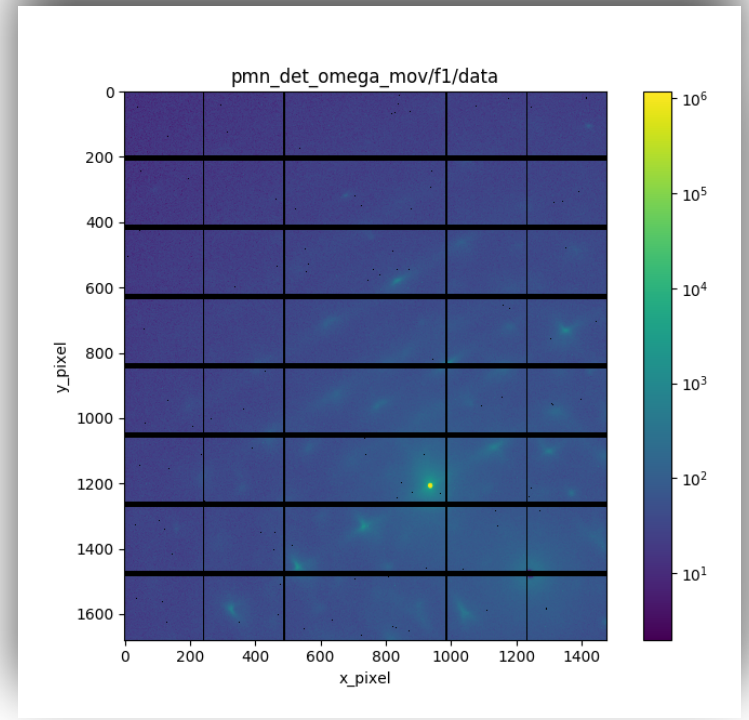

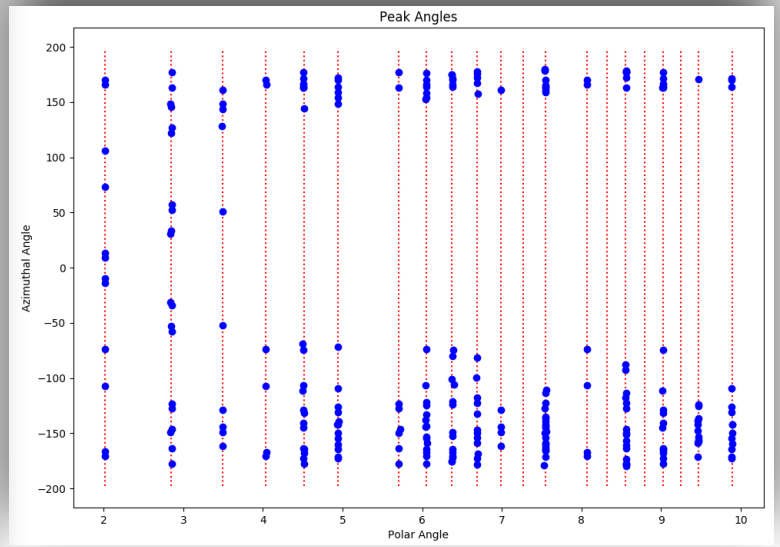

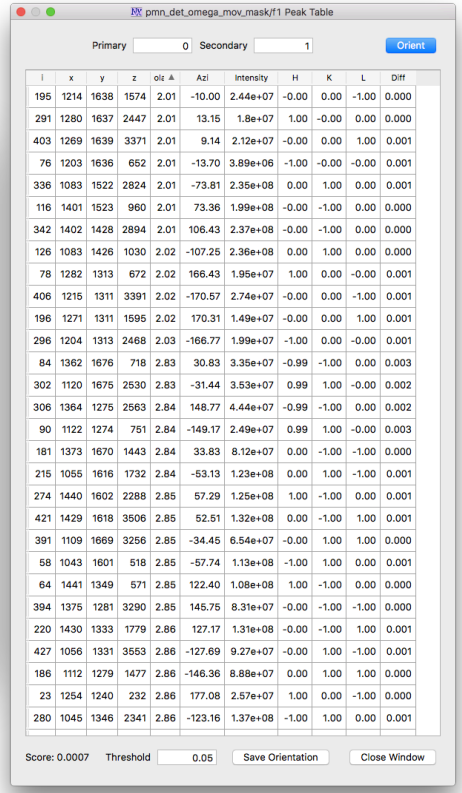

I	x	y	z	ole	Azi	Intensity	H	K	L	Diff
195	1214	1638	1574	2.01	-10.00	2.44e+07	-0.00	0.00	-1.00	0.000
291	1280	1637	2447	2.01	13.15	1.8e+07	1.00	-0.00	0.00	0.000
403	1269	1639	3371	2.01	9.14	2.12e+07	-0.00	0.00	1.00	0.001
76	1203	1636	652	2.01	-13.70	3.89e+06	-1.00	-0.00	-0.00	0.001
336	1083	1522	2824	2.01	-73.81	2.35e+08	0.00	1.00	0.00	0.001
116	1401	1523	960	2.01	73.36	1.99e+08	-0.00	-1.00	0.00	0.000
342	1402	1428	2894	2.01	106.43	2.37e+08	-0.00	-1.00	0.00	0.000
126	1083	1426	1030	2.02	-107.25	2.36e+08	0.00	1.00	0.00	0.000
78	1282	1313	672	2.02	166.43	1.95e+07	1.00	0.00	-0.00	0.001
406	1215	1311	3391	2.02	-170.57	2.74e+07	-0.00	0.00	-1.00	0.001
196	1271	1311	1595	2.02	170.31	1.49e+07	-0.00	0.00	1.00	0.001
296	1204	1313	2468	2.03	-166.77	1.99e+07	-1.00	0.00	-0.00	0.001
84	1362	1676	718	2.83	30.83	3.35e+07	-0.99	-1.00	0.00	0.003
302	1120	1675	2530	2.83	-31.44	3.53e+07	0.99	1.00	-0.00	0.002
306	1364	1275	2563	2.84	148.77	4.44e+07	-0.99	-1.00	0.00	0.002
90	1122	1274	751	2.84	-149.17	2.49e+07	0.99	1.00	-0.00	0.003
181	1373	1670	1443	2.84	33.83	8.12e+07	0.00	-1.00	-1.00	0.000
215	1055	1616	1732	2.84	-53.13	1.23e+08	0.00	1.00	-1.00	0.001
274	1440	1602	2288	2.85	57.29	1.25e+08	1.00	-1.00	0.00	0.001
421	1429	1618	3506	2.85	52.51	1.32e+08	0.00	-1.00	1.00	0.001
391	1109	1669	3256	2.85	-34.45	6.54e+07	-0.00	1.00	1.00	0.000
58	1043	1601	518	2.85	-57.74	1.13e+08	-1.00	1.00	0.00	0.001
64	1441	1349	571	2.85	122.40	1.08e+08	1.00	-1.00	0.00	0.000
394	1375	1281	3290	2.85	145.75	8.31e+07	-0.00	-1.00	-1.00	0.000
220	1430	1333	1779	2.86	127.17	1.31e+08	-0.00	-1.00	1.00	0.001
427	1056	1331	3553	2.86	-127.69	9.27e+07	-0.00	1.00	-1.00	0.001
186	1112	1279	1477	2.86	-146.36	8.88e+07	0.00	1.00	1.00	0.000
23	1254	1240	232	2.86	177.08	2.57e+07	1.00	0.00	-1.00	0.000
280	1045	1346	2341	2.86	-123.16	1.37e+08	-1.00	1.00	0.00	0.001

DIFFUSE SCATTERING IN 3D
THE RELAXOR $PbMg_{1/3}Nb_{2/3}O_3$

M. J. Krogstad, *et al*, Nature Materials **48**, 1 (2018).

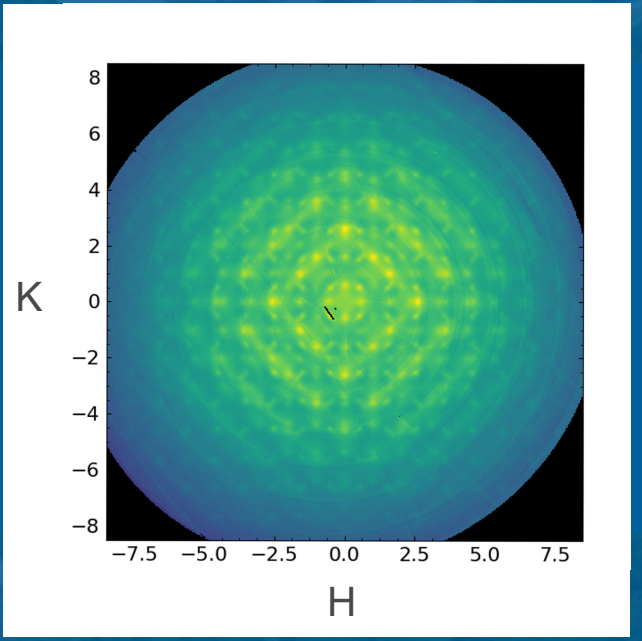

DIFFUSE GALLERY

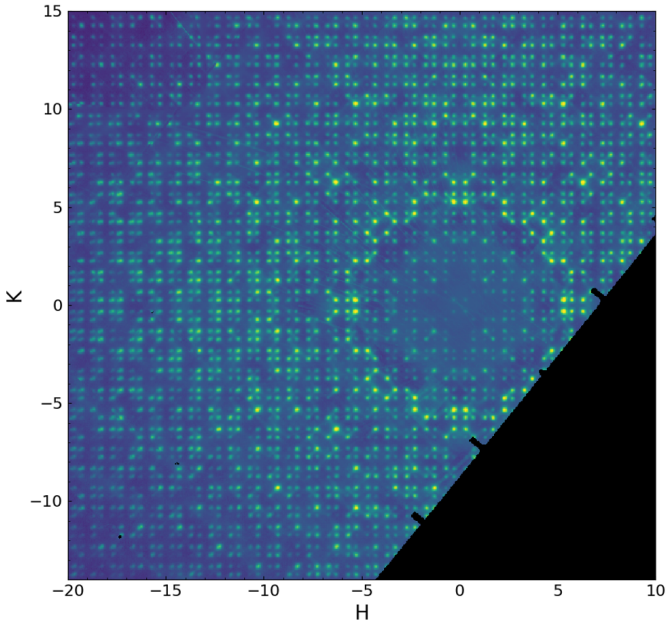

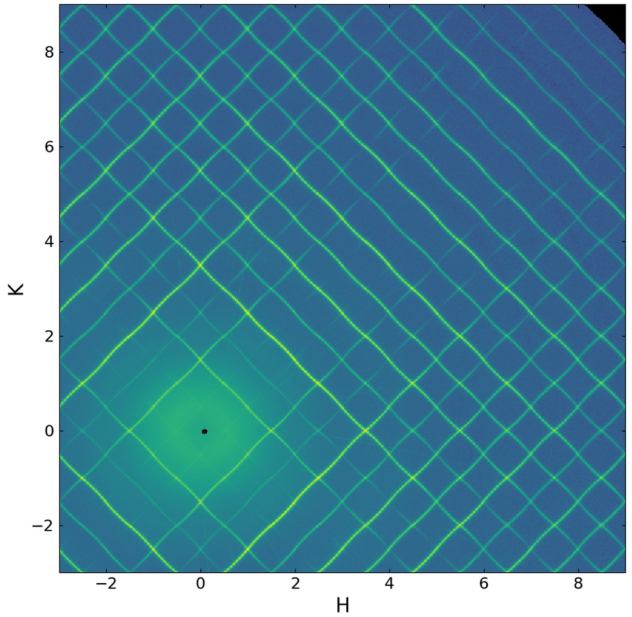

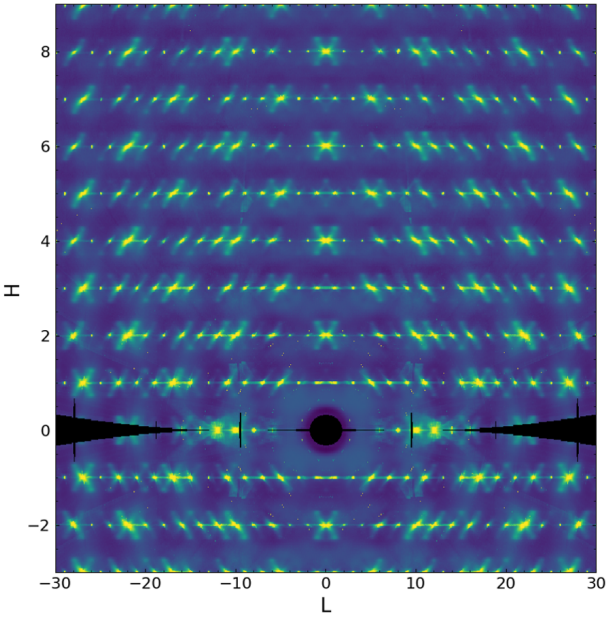

CASE STUDY 1: MULLITE

MULLITE - A CASE STUDY

B. D. Butler, T. R. Welberry, & R. L. Withers, Phys Chem Minerals **20**, 323 (1993)

- Mullite is a ceramic that is formed by adding O^{2+} vacancies to Sillimanite
  - Sillimanite has alternating AlO_4 and SiO_4 tetrahedra
  - Mullite has excess Al^{3+} occupying Si^{2+} sites for charge balance
- This results in strong vacancy-vacancy correlations

AlO_6 Octahedra

SiO_4 Tetrahedra

AlO_4 Tetrahedra

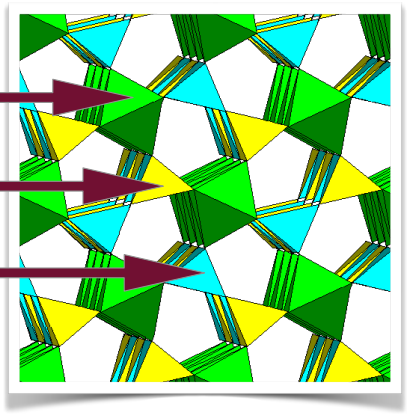

Sillimanite: Al_2SiO_5

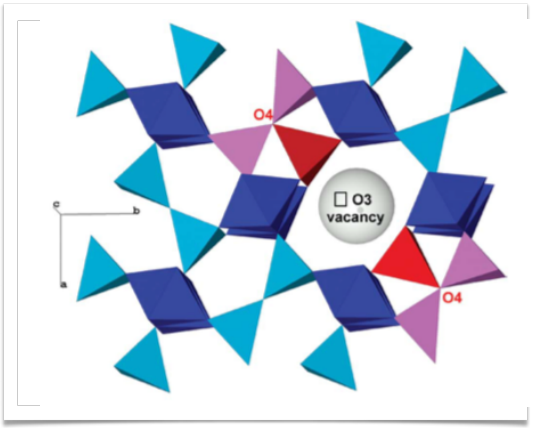

Mullite: $Al_2(Al_{2+2x}Si_{2-2x})O_{10-x}$

3D DIFFUSE SCATTERING IN MULLITE

- There is strong diffuse scattering throughout reciprocal space
- The shape of the diffuse scattering is strongly dependent on the value of L

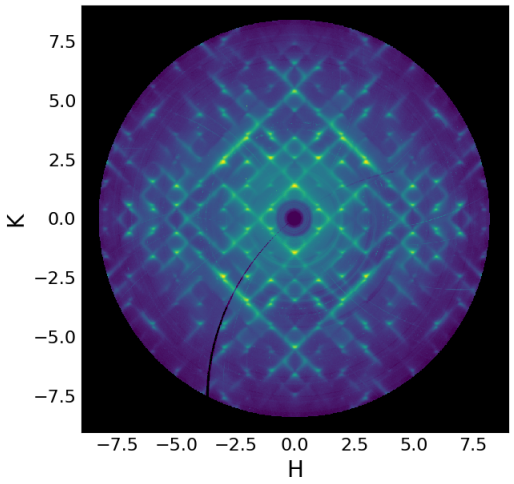

L=0.16

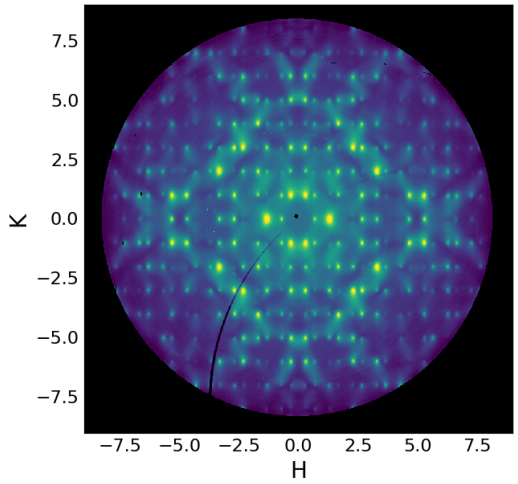

L=0.5

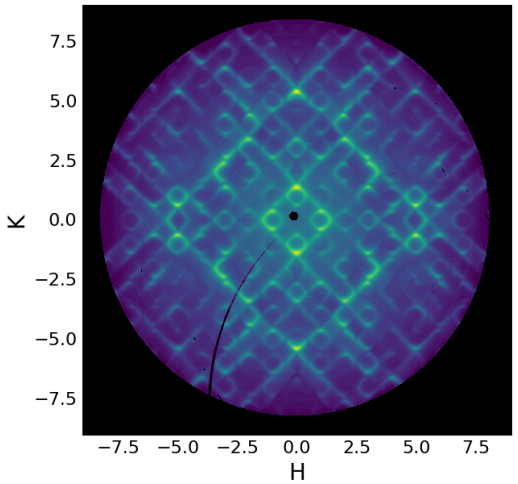

L=0.75

MONTE CARLO ANALYSIS

B. D. Butler, T. R. Welberry, & R. L. Withers,
Phys Chem Minerals **20**, 323 (1993)

- In a classic analysis, Richard Welberry and colleagues developed a set of interaction energies to model mullite disorder
- Interaction energies were initialized:
  - insights from chemical intuition
  - insights from the measured diffuse scattering
- The diffuse scattering was calculated using a Monte Carlo algorithm to generate vacancy distributions first in 2D slices and then in 3D

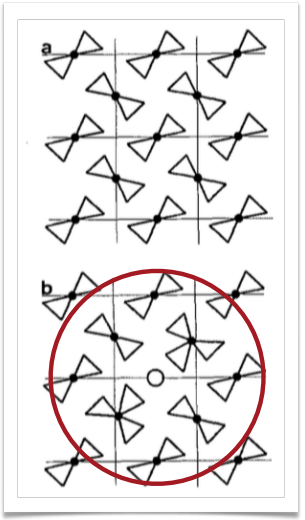

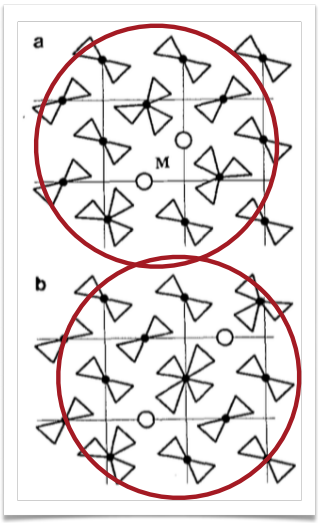

Interatomic vector	α_{lmn}	Interatomic vector	α_{lmn}
$\frac{1}{2}\langle 1\,1\,0\rangle$	−0.24	$\langle 0\,2\,0\rangle$	+0.13
$[1\,1\,0]$	−0.23	$\frac{1}{2}\langle 3\,1\,0\rangle$	+0.22
$[1\,-1\,0]$	−0.05	$\frac{1}{2}\langle 1\,3\,0\rangle$	−0.01
$\langle 1\,0\,0\rangle$	−0.06	$\langle 1\,0\,1\rangle$	+0.07
$\langle 0\,1\,0\rangle$	+0.22	$\langle 0\,1\,1\rangle$	−0.12
$\langle 0\,0\,1\rangle$	−0.03	$\frac{1}{2}\langle 3\,3\,0\rangle$	+0.17
$\frac{1}{2}[1\,-1\,2]$	+0.12	$\langle 1\,1\,1\rangle$	−0.01
$\frac{1}{2}[1\,1\,2]$	+0.12	$\frac{1}{2}\langle 3\,1\,2\rangle$	−0.11
$\langle 2\,0\,0\rangle$	−0.12	$\frac{1}{2}\langle 3\,3\,2\rangle$	−0.07

MONTE CARLO ANALYSIS RESULTS

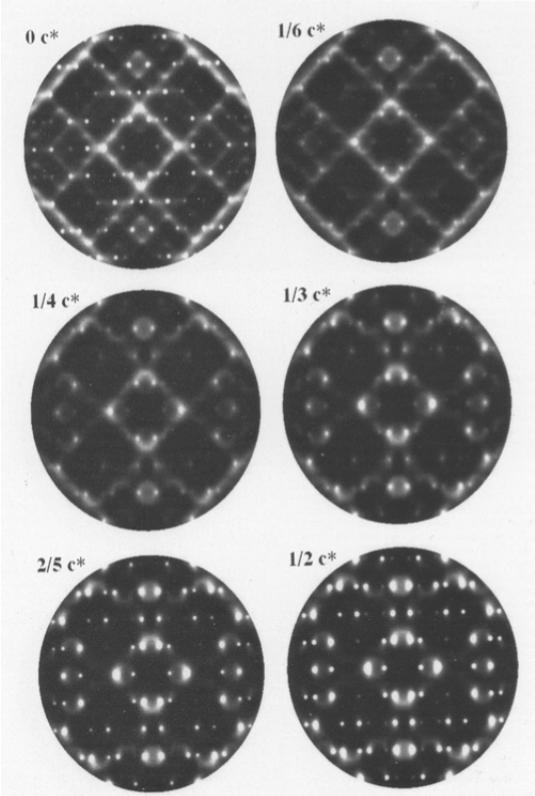

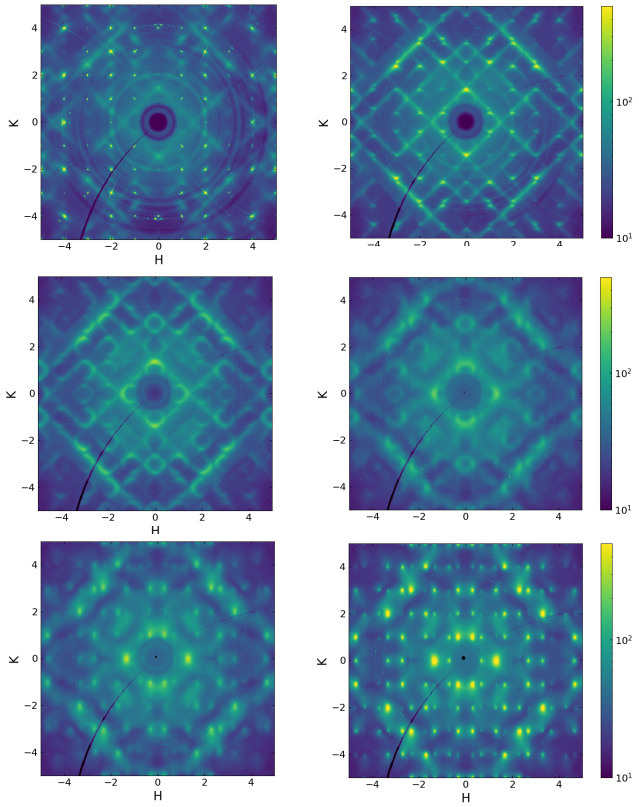

VACANCY ORDERING IN MULLITE

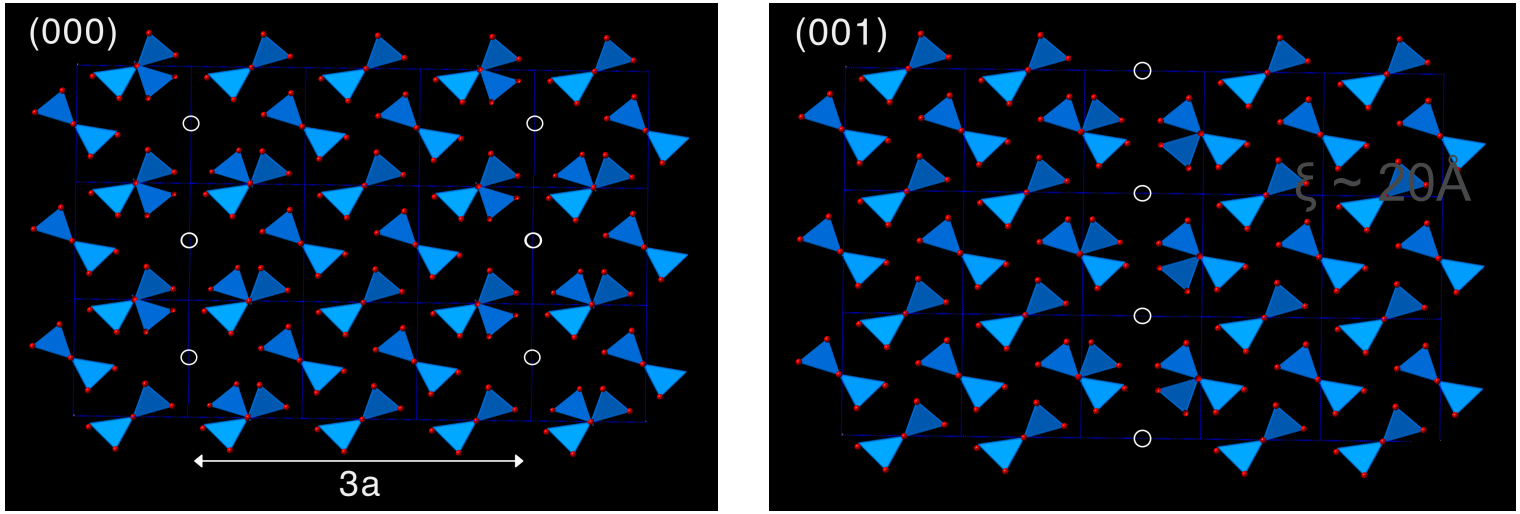

c = 0

$$\mathbf{q} = \pm\frac{1}{2}\mathbf{c}^* \pm \frac{1}{3}\mathbf{a}^*$$

c = 1.0

CASE STUDY 2: SODIUM-INTERCALATED V_2O_5 3D-ΔPDF

PAIR DISTRIBUTION FUNCTION ANALYSIS

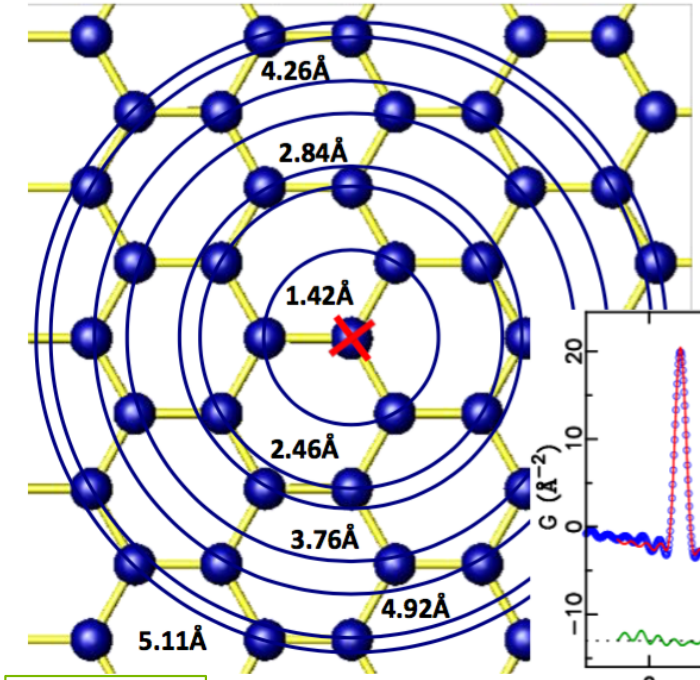

Radial atomic **p**air **d**istribution function (PDF) gives the interatomic distance distribution, or "probability" of finding atomic pairs distance *r* apart

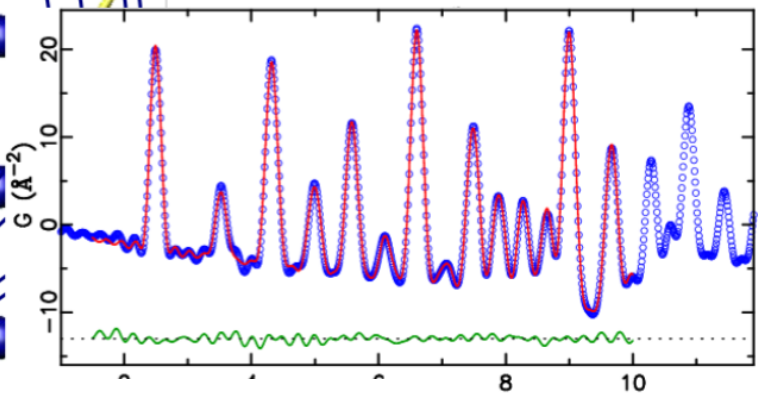

$$G(r) = 4\pi r[\rho(r) - \rho_o] = (2/\pi) \int_{Q=Q_{min}}^{Q_{max}} Q[S(Q) - 1]\sin(Qr)dQ$$

Emil Bozin (ADD 2013)

THREE-DIMENSIONAL PAIR DISTRIBUTION FUNCTIONS

238 Z. Kristallogr. 2012, 227, 238–247 / DOI 10.1524/zkri.2012.1504

The three-dimensional pair distribution function analysis of disordered single crystals: basic concepts

Thomas Weber* and Arkadiy Simonov

Laboratory of Crystallography, ETH Zurich Wolfgang-Pauli-Str. 10, 8093 Zurich, Switzerland

- The 3D PDF technique was pioneered by Thomas Weber and colleagues at ETH
  - Philippe Schaub, Walter Steurer, Arkadiy Simonov
  - See *Yell* - A. Simonov, *et al*, J Appl Cryst **47**, 1146 (2014).
- The ability to measure three-dimensional S(**Q**) over a large volume of reciprocal space provides the 3D analog of PDF measurements.
  - Total PDFs if Bragg peaks and diffuse scattering can be measured simultaneously
  - ΔPDFs if the Bragg peaks are eliminated
- This allows a model-independent view of the measurements in real space.

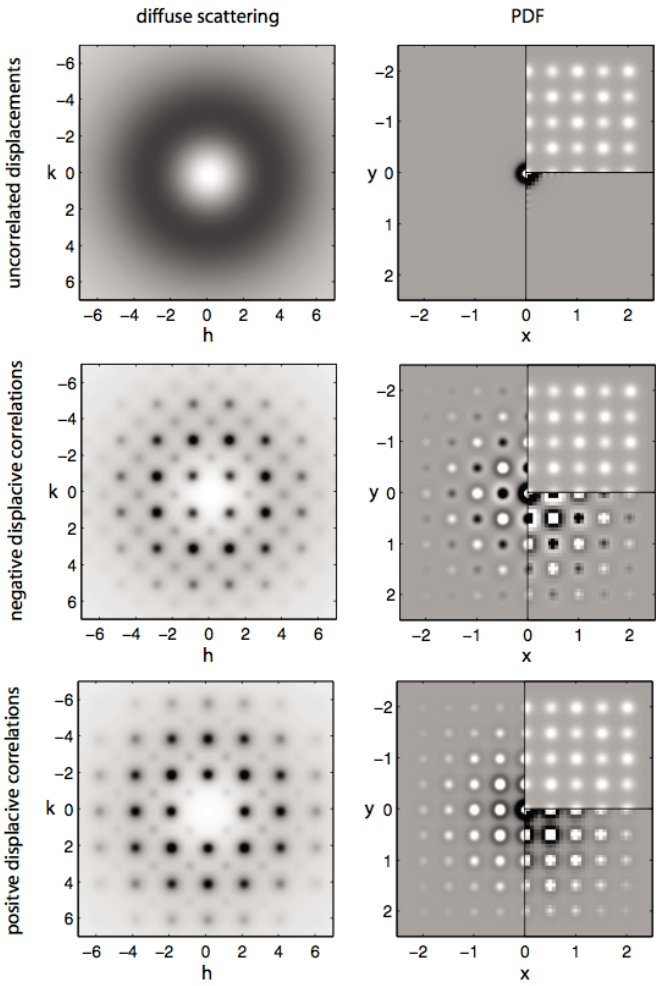

“PUNCH AND FILL”

$$I = \sum_i \sum_j b_i b_j \exp(i\mathbf{Q} \cdot \mathbf{r}_{ij}) \qquad P_{tot}(\mathbf{r}) = FT\left[I(\mathbf{Q})\right] = FT\left[|\bar{F}(\mathbf{Q})|^2\right] + FT\left[|\Delta F(\mathbf{Q})|^2\right] = P_{hkl}(\mathbf{r}) + \Delta P(\mathbf{r})$$

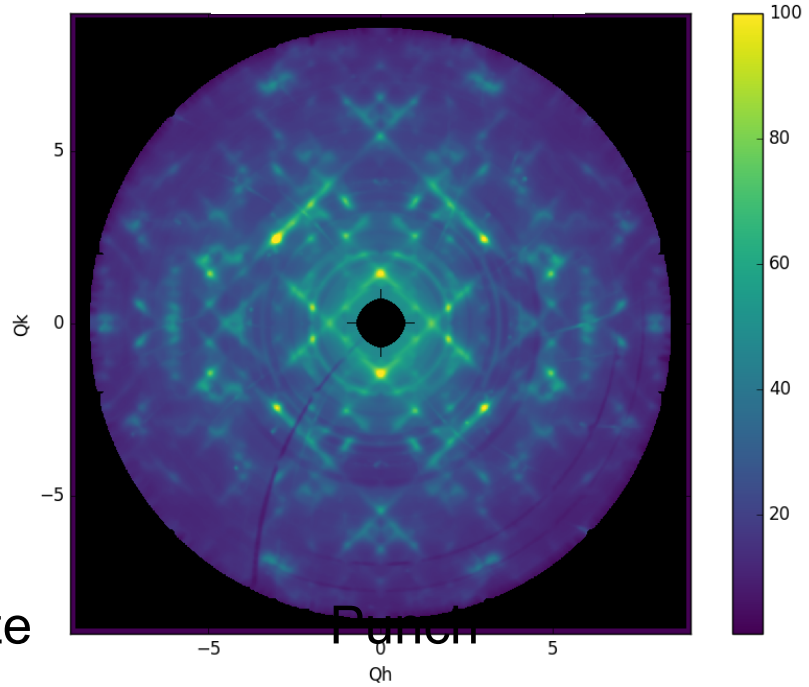

Symmetrize Punch Fill

A. Simonov, T. Weber, and W. Steurer, Journal of Applied Crystallography **47**, 1146 (2014).

SODIUM-INTERCALATED V_2O_5

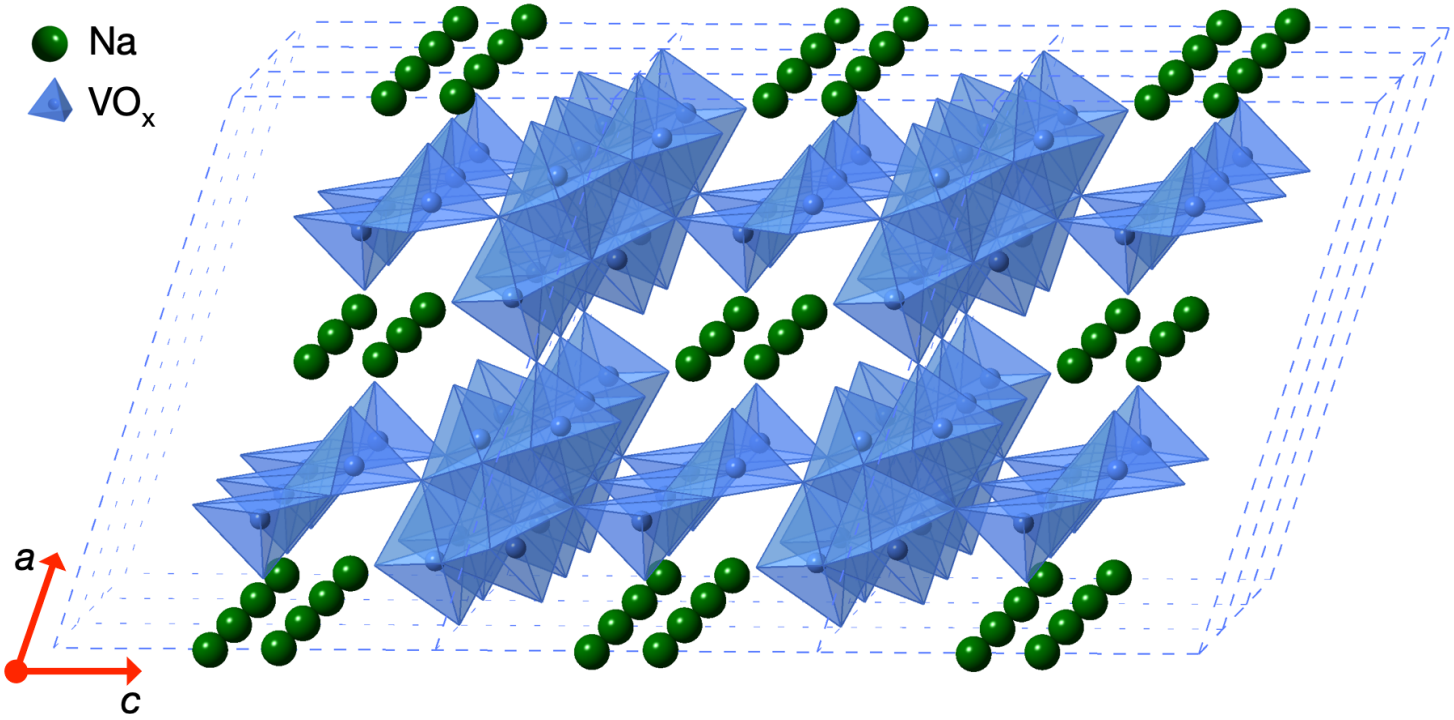

M. J. Krogstad, S. Rosenkranz, J. M. Wozniak, G. Jennings, J. P. C. Ruff, J. T. Vaughey, and R. Osborn
Nature Materials **19**, 63 (2020).

SUBLATTICE MELTING IN $Na_{0.45}V_2O_5$

Order-Disorder Transition in the Half-Filled Sodium Sublattice

K=0.5

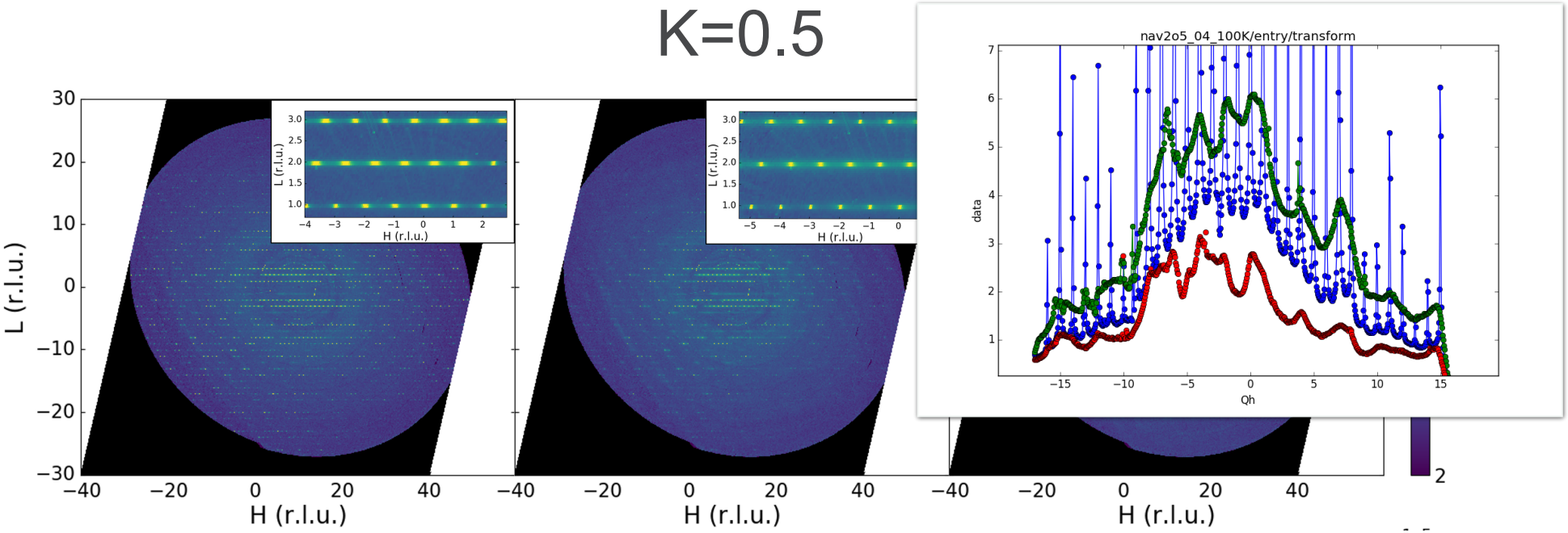

50K 200K 250K

3D-ΔPDF ANALYSIS OF $Na_{0.45}V_2O_5$

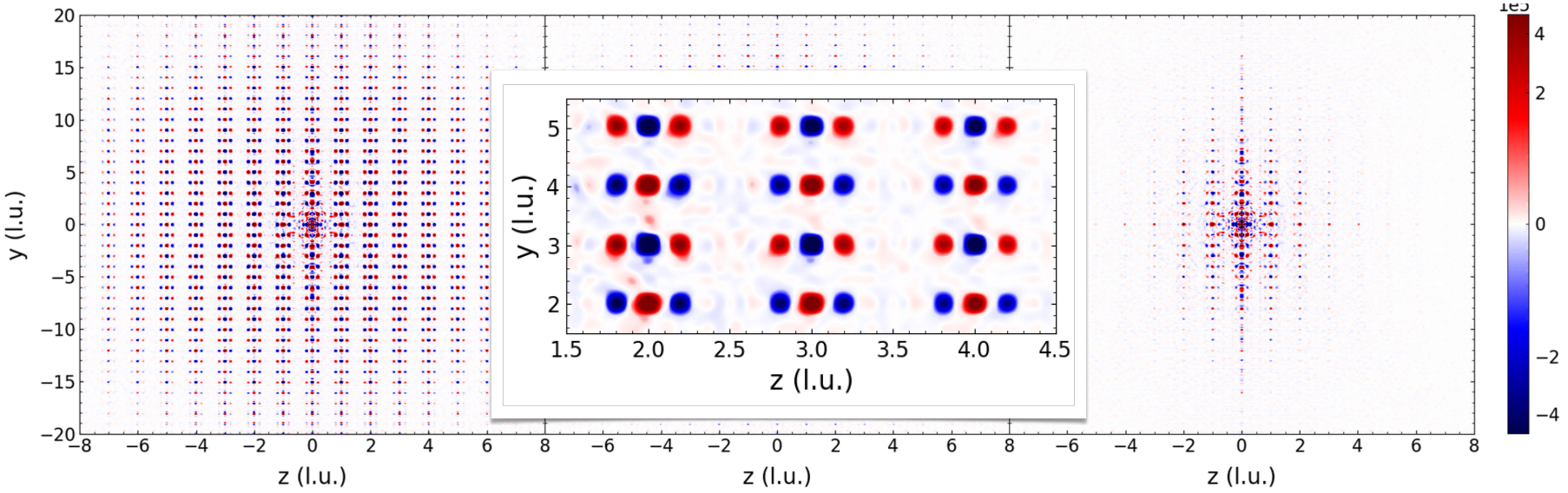

50K 200K 250K

3D-ΔPDF ANALYSIS OF $Na_{0.45}V_2O_5$

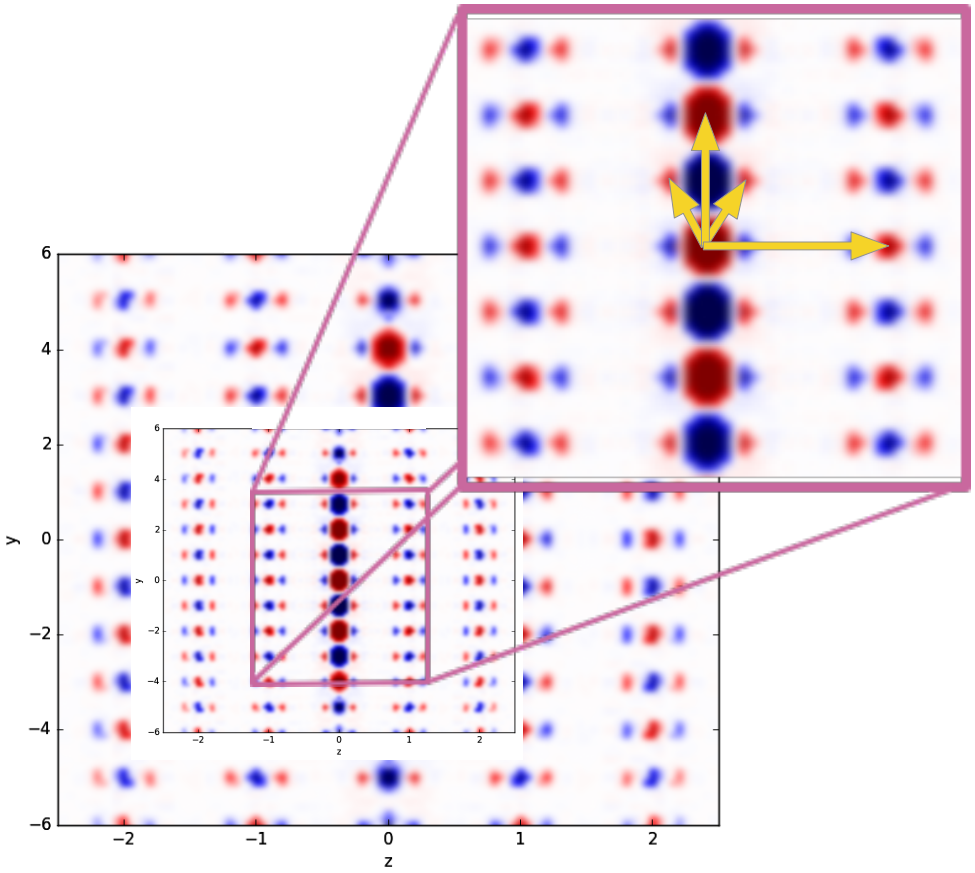

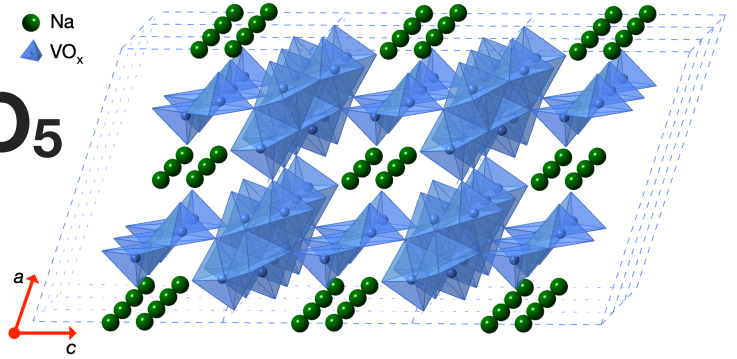

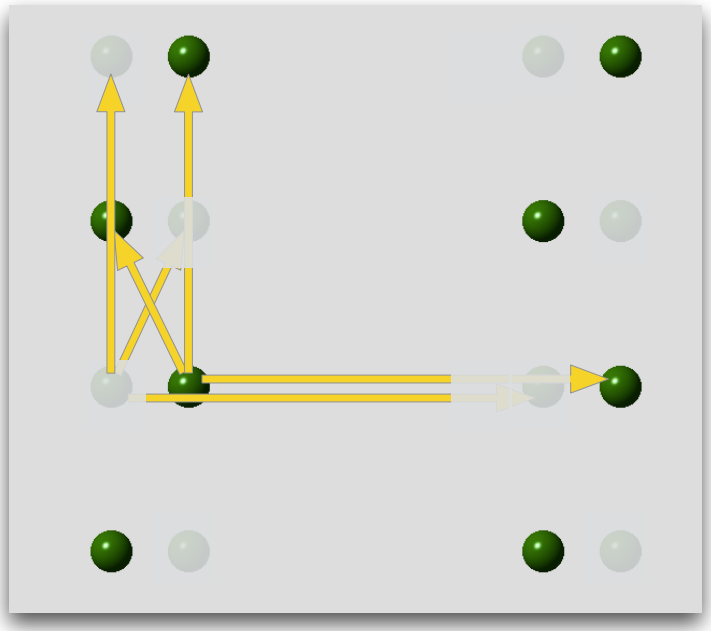

REAL SPACE *vs* 3D–ΔPDF

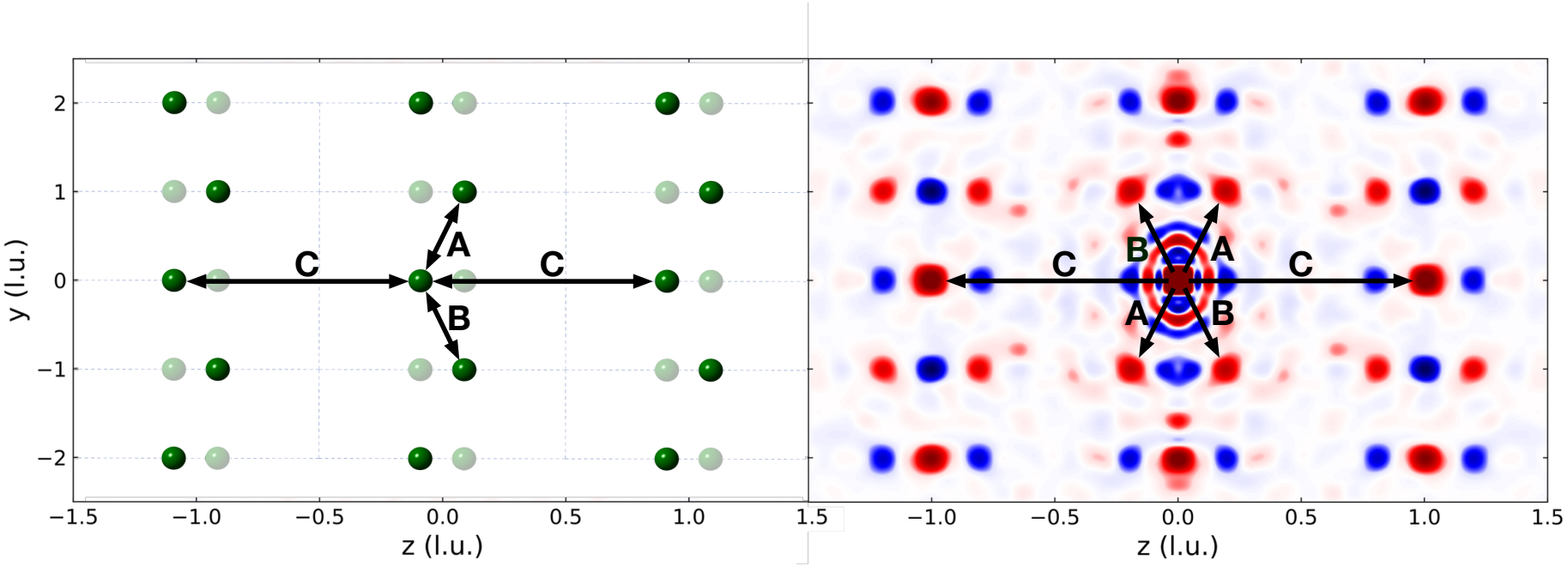

ORDER-DISORDER TRANSITION VIEWED IN REAL SPACE

$Na_{0.45}V_2O_5$

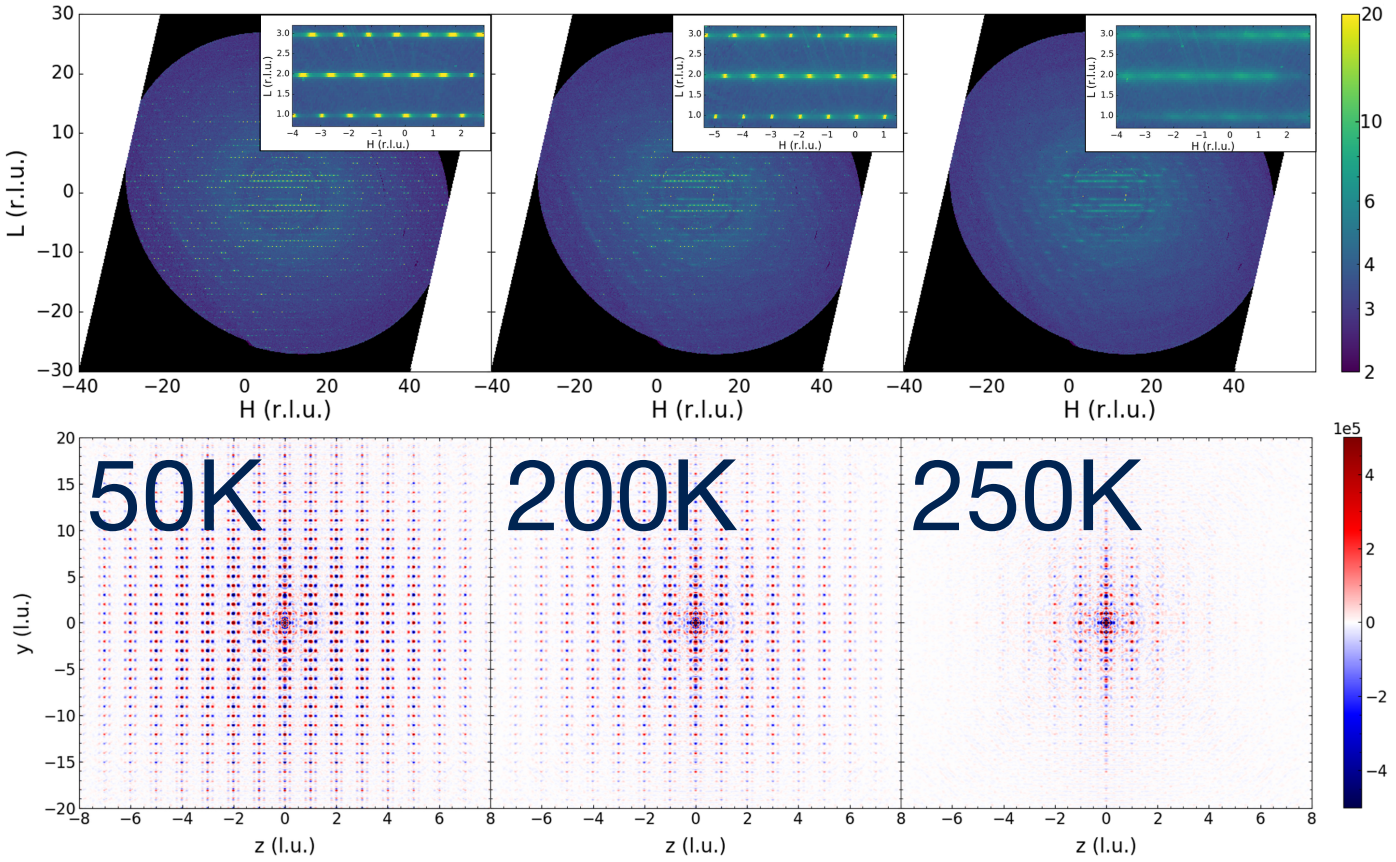

EFFECT OF Q-RESOLUTION

- Finite Q-resolution ➡ Gaussian envelope in real space.
- The width can be determined from the total PDF
  - *i.e.*, the transform of the long-range crystal structure.

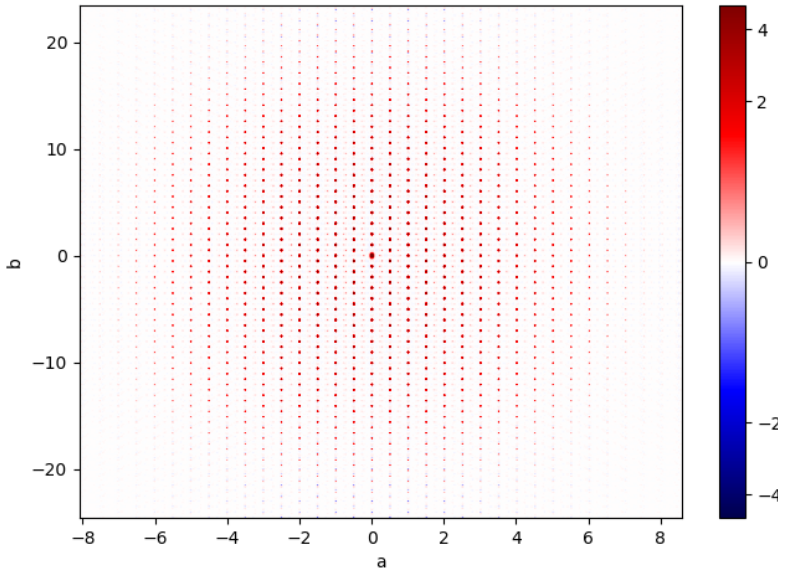

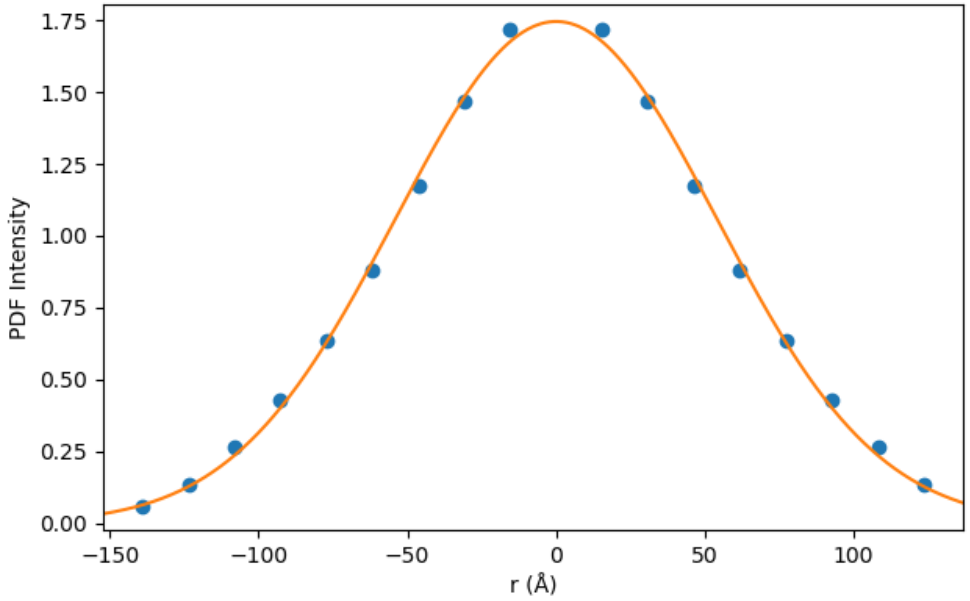

FITTING CORRELATION LENGTHS IN REAL SPACE

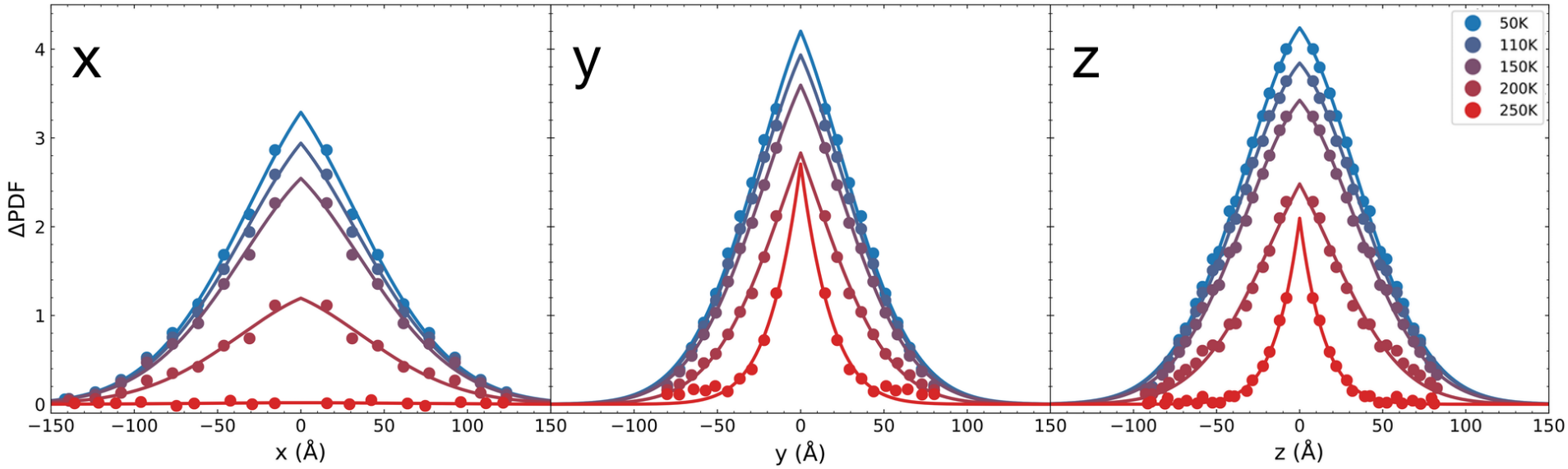

$$f(\mathbf{r}) = A \times G(\mathbf{r}) \times \exp(-|\mathbf{r}|/\xi)$$

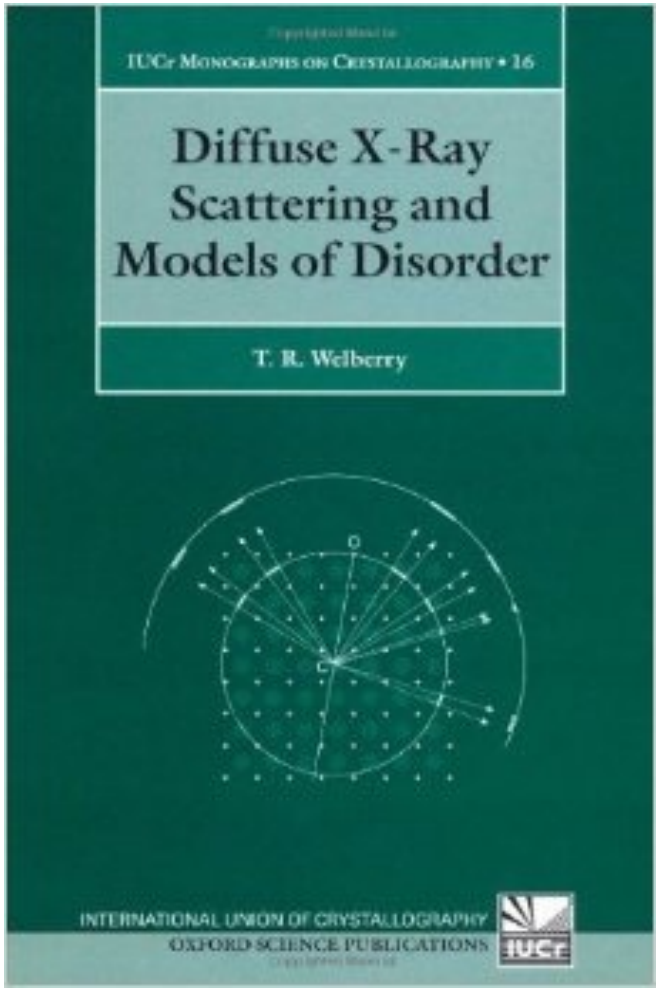

24.3.3 *Ordering of Na within the two-leg ladders.*

Fig. 24.10(a) shows a small region near the origin of the x = 0 plane of the ΔPDF map obtained from the 50K X-ray data. The strong white origin peak indicates perfect positive correlation for an atom with itself. Other white peaks also indicate a positive correlation between an atom at the origin with another at a position given by the vectors A, B or C (and the reverse vectors -A, -B and -C). Conversely the dark peaks indicate strong negative correlations. It is quite straightforward to deduce from the observed pattern of white and dark peaks that the local arrangement of the Na ions must follow a pattern like that shown in Fig. 24.10(b), where the occupancy of the two Na sites on each rung of the two-leg ladders tends to alternate between (Na□[†]) and (□Na) producing a zig-zag chain of occupied sites. Neighbouring ladders at $z = \pm 1.0$ have the same occupancy pattern which is in phase with the ladder at $z = 0$.

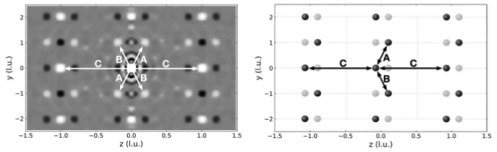

Fig. 24.10 A comparison of (a) the ΔPDF peak intensities at 50K in the $x = 0$ plane of $Na_{0.45}V_2O_5$ with (b) the derived real-space model of sodium ions. Data used in this figure are reproduced with kind permission of Dr Ray Osborn.

24.3.4 *ΔPDF peak intensities in the $z = 0$ plane.*

Fig. 24.12 shows the $z = 0$ plane of the ΔPDF map observed at three different temperatures. Fig. 24.11(b) shows an enlargement of part of Fig. 24.11(a) where white arrows (labelled A –F) have been used to identify different interatomic vectors. The same set of vectors is shown in Fig. 24.11(e) which is a plot of the $z = 0$ plane of the average structure. The maps are dominated by the same alternating correlations of Na occupancy along the ladder direction parallel to y. Similarly neighbouring chains at $x = \pm 1$ are instep with that at $x = 0$ for temperatures 50K and 150K but at 250K these correlations have been lost.

Although the maps are dominated by the correlations in the Na ladders there are numerous weaker peaks that correspond to correlations between the ladder Na_1 ions and the interstitial Na_2 ions. These correspond to vectors A, B, C and E in Fig. 24.11(e) and involve one Na_1 and one Na_2 ion. These peaks are clearly evident in the 50K map, somewhat less evident at 150K and even less evident at 250K. They are weak relative to those involving Na_1 ions alone simply because of the low occupancy of the Na_2 sites.

[†]here □ is used to represent a vacant site

BACK TO MULLITE

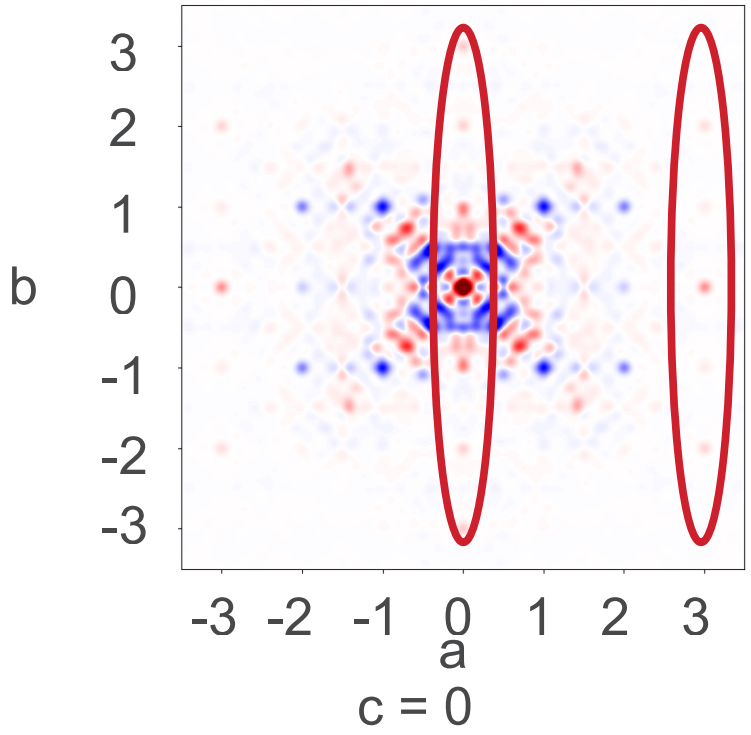

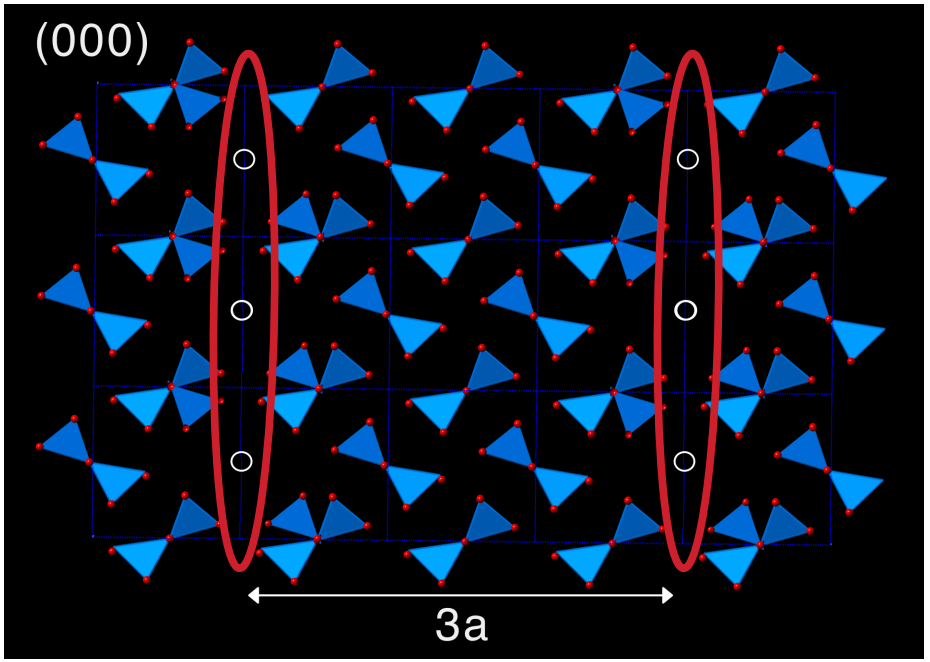

HOW DO I LOOK AT STATIC DISORDER?

COMPARISON OF ELASTIC SCATTERING AND THE STATIC APPROXIMATION

$$G(\mathbf{r},t) = \frac{1}{N}\left\langle \sum_{i=1}^{N}\sum_{j=1}^{N} \delta(\mathbf{r} - \mathbf{r}_i(t) + \mathbf{r}_j(0))\right\rangle$$

$$S(\mathbf{Q},\omega) = \frac{1}{N}\frac{1}{2\pi\hbar}\int_{\infty}^{\infty} e^{-i\omega t}dt \int G(\mathbf{r},t)e^{-i\mathbf{Q}\cdot\mathbf{r}}d\mathbf{r} \qquad \hbar\delta(t) = \frac{1}{2\pi}\int_{-\infty}^{\infty} e^{i\omega t}d(\hbar\omega)$$

$$\left(\frac{d\sigma}{d\Omega}\right)_{coh}^{static} = b_{coh}^2 N \int G(\vec{r},0)e^{i\vec{Q}.\vec{r}}d\vec{r}$$

$$\left(\frac{d\sigma}{d\Omega}\right)_{coh}^{elastic} = b_{coh}^2 N \int G(\vec{r},\infty)e^{i\vec{Q}.\vec{r}}d\vec{r}$$

MEASURING LARGE VOLUMES OF RECIPROCAL SPACE

Conventional Time-of-Flight Neutron Methods

White Beam:
efficient

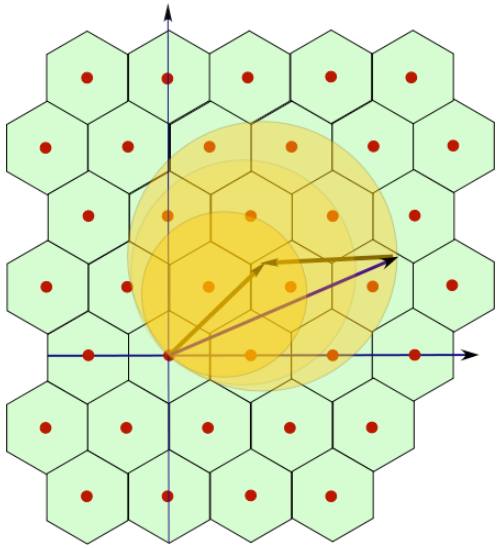

NO energy discrimination

Fixed ki :
energy resolved

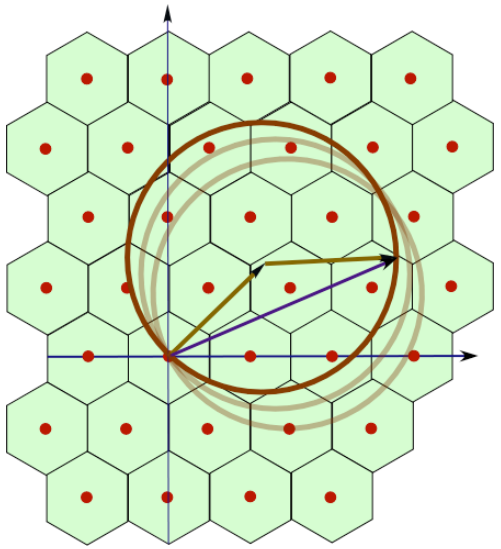

NOT efficient

CROSS CORRELATION CHOPPER

S. Rosenkranz and R. Osborn, PRAMANA- Journal of Physics, **71**, 705 (2008).

TOF Laue Diffractometer
- highly efficient data collection
- wide dynamic range in Q

Statistical Chopper
- elastic energy discrimination
- optimum use of white beam

Elastic scattering: $\hbar\omega = 0$

Inelastic scattering: $\hbar\omega = +E_0$

$\hbar\omega = -E_0$

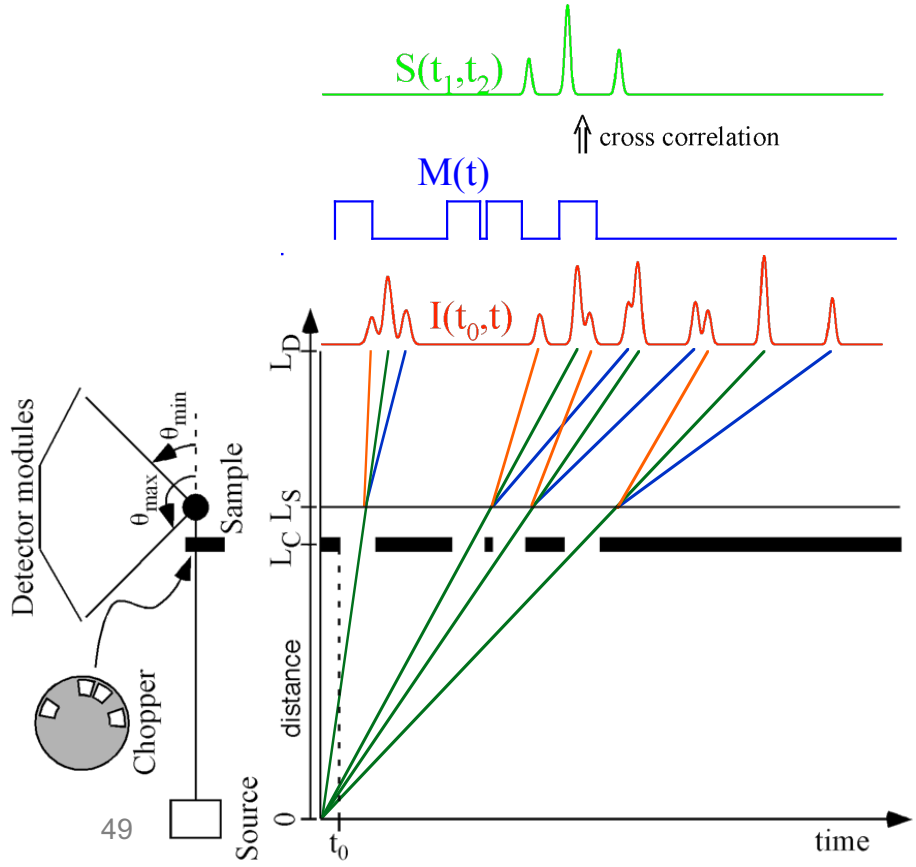

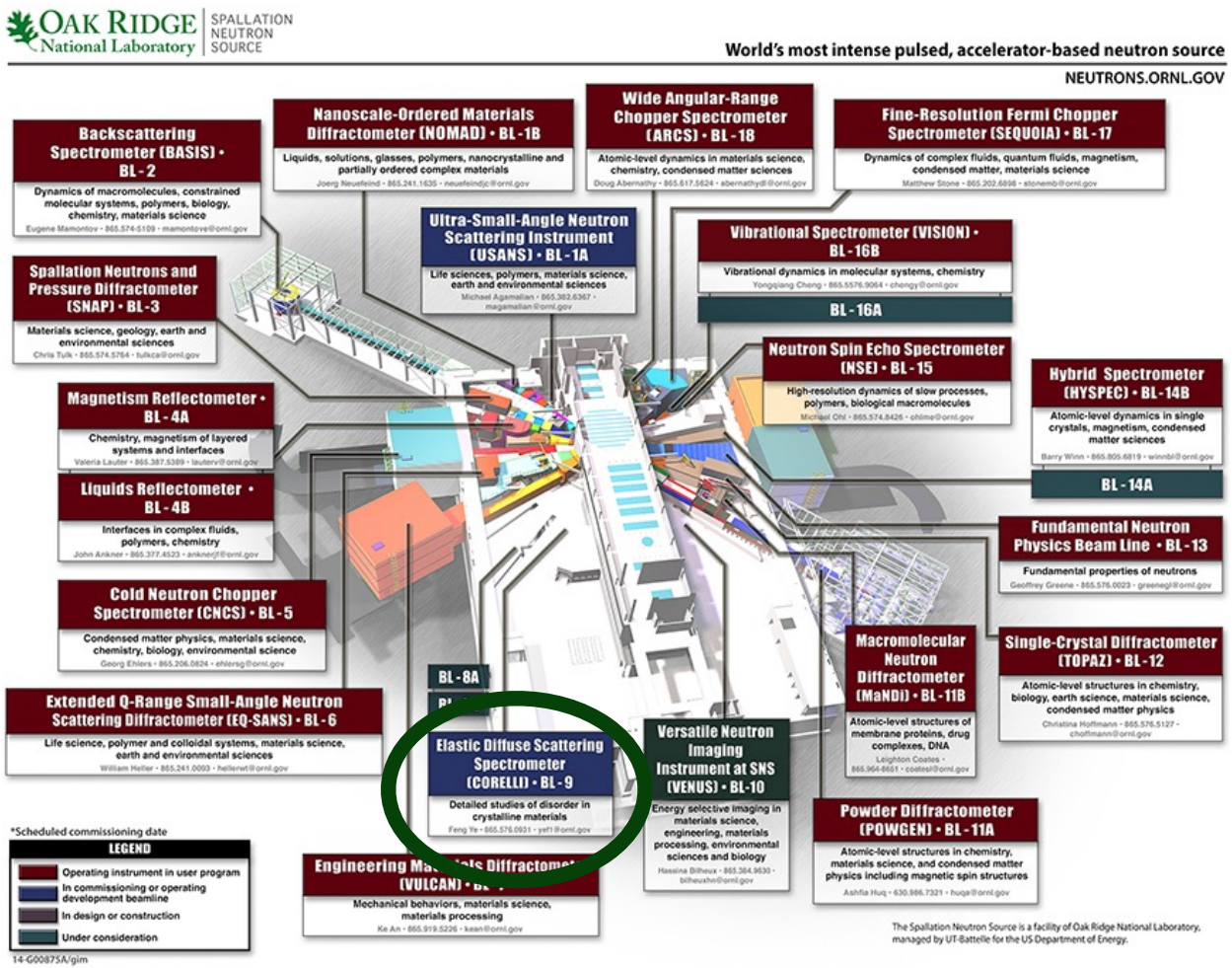
OAK RIDGE National Laboratory | SPALLATION NEUTRON SOURCE
World's most intense pulsed, accelerator-based neutron source
NEUTRONS.ORNL.GOV
Backscattering Spectrometer (BASIS) • BL-2
Dynamics of macromolecules, constrained molecular systems, polymers, biology, chemistry, materials science
Nanoscale-Ordered Materials Diffractometer (NOMAD) • BL-1B
Liquids, solutions, glasses, polymers, nanocrystalline and partially ordered complex materials
Wide Angular-Range Chopper Spectrometer (ARCS) • BL-18
Atomic-level dynamics in materials science, chemistry, condensed matter sciences
Fine-Resolution Fermi Chopper Spectrometer (SEQUOIA) • BL-17
Dynamics of complex fluids, quantum fluids, magnetism, condensed matter, materials science
Ultra-Small-Angle Neutron Scattering Instrument (USANS) • BL-1A
Life sciences, polymers, materials science, earth and environmental sciences
Vibrational Spectrometer (VISION) • BL-16B
Vibrational dynamics in molecular systems, chemistry
BL-16A
Spallation Neutrons and Pressure Diffractometer (SNAP) • BL-3
Materials science, geology, earth and environmental sciences
Neutron Spin Echo Spectrometer (NSE) • BL-15
High-resolution dynamics of slow processes, polymers, biological macromolecules
Hybrid Spectrometer (HYSPEC) • BL-14B
Atomic-level dynamics in single crystals, magnetism, condensed matter sciences
BL-14A
Magnetism Reflectometer • BL-4A
Chemistry, magnetism of layered systems and interfaces
Liquids Reflectometer • BL-4B
Interfaces in complex fluids, polymers, chemistry
Fundamental Neutron Physics Beam Line • BL-13
Fundamental properties of neutrons
Cold Neutron Chopper Spectrometer (CNCS) • BL-5
Condensed matter physics, materials science, chemistry, biology, environmental science
Macromolecular Neutron Diffractometer (MaNDI) • BL-11B
Atomic-level structures of membrane proteins, drug complexes, DNA
Single-Crystal Diffractometer (TOPAZ) • BL-12
Atomic-level structures in chemistry, biology, earth science, materials science, condensed matter physics
BL-8A
Extended Q-Range Small-Angle Neutron Scattering Diffractometer (EQ-SANS) • BL-6
Life science, polymer and colloidal systems, materials science, earth and environmental sciences
Elastic Diffuse Scattering Spectrometer (CORELLI) • BL-9
Detailed studies of disorder in crystalline materials
Versatile Neutron Imaging Instrument at SNS (VENUS) • BL-10
Energy selective imaging in materials science, engineering, materials processing, environmental sciences and biology
Powder Diffractometer (POWGEN) • BL-11A
Atomic-level structures in chemistry, materials science, and condensed matter physics including magnetic spin structures
Engineering Materials Diffractometer (VULCAN) • BL-
Mechanical behaviors, materials science, materials processing
*Scheduled commissioning date
LEGEND
Operating instrument in user program
In commissioning or operating development beamline
In design or construction
Under consideration
14-G00875A/gim
The Spallation Neutron Source is a facility of Oak Ridge National Laboratory, managed by UT-Battelle for the US Department of Energy.

CORELLI

<u>Instrument Scientists</u>
Feng Ye
Yaohua Liu

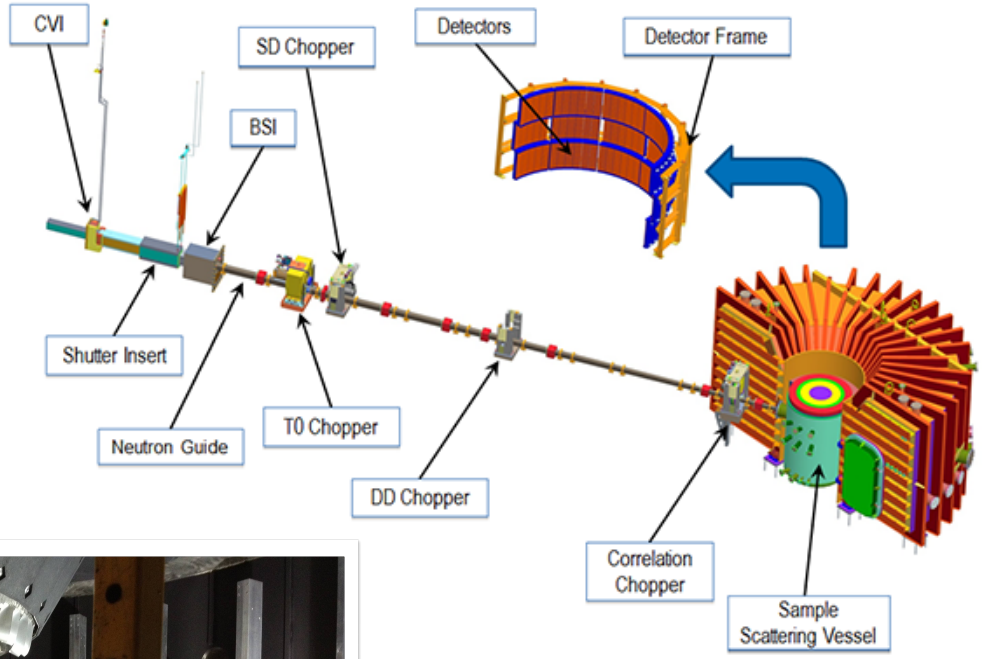

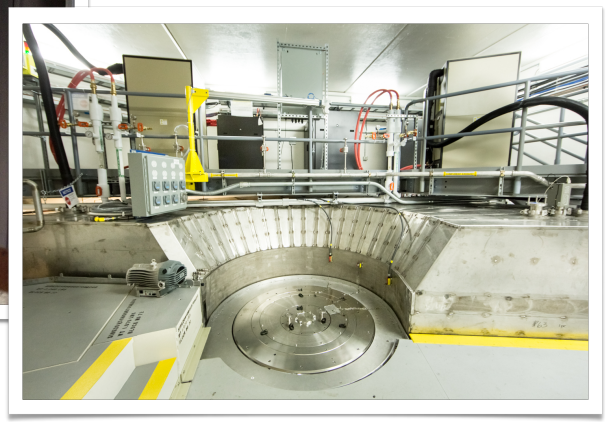

<u>Instrument Proposers</u>
Stephan Rosenkranz
Ray Osborn

CROSS CORRELATION IN ACTION

Raw Data

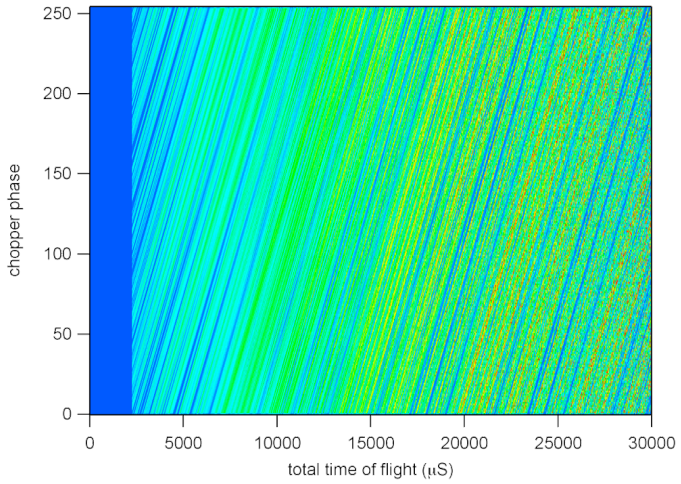

Cross Correlation

Reconstructed Scattering Function

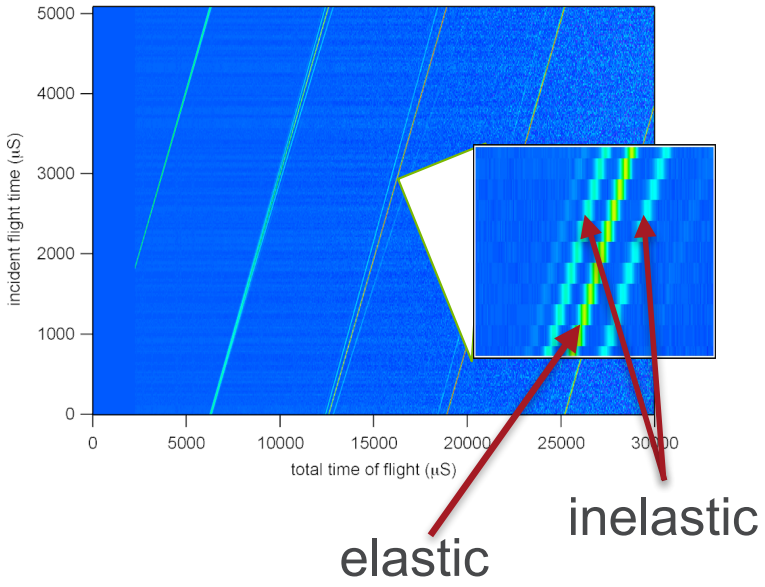

ELASTIC DISCRIMINATION WITH CROSS CORRELATION

Benzil $C_{14}H_{10}O_2$

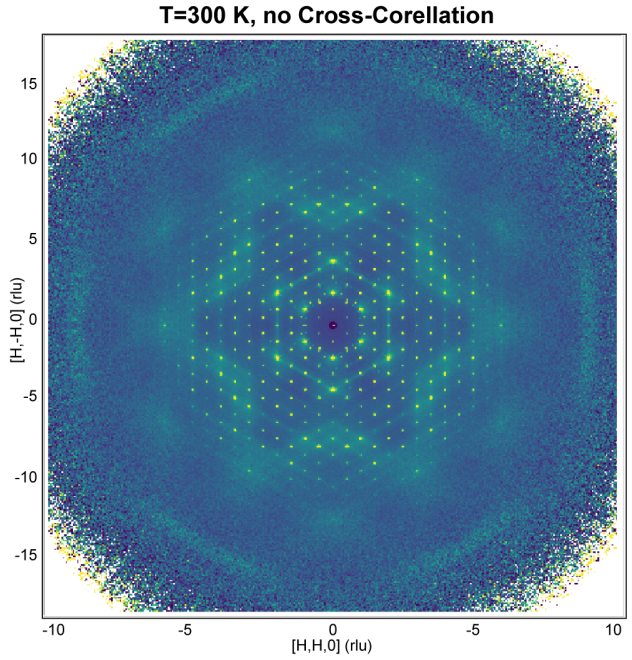

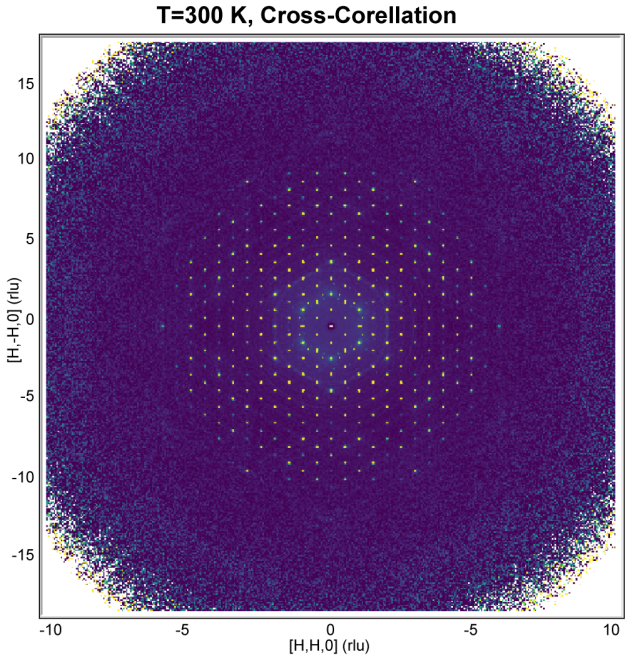

T. R. Welberry and R. Whitfield, Quantum Beam Science **2**, 2 (2018)

DIFFUSE SCATTERING FROM A FAST-ION CONDUCTOR

Sublattice Melting in $SrCl_2$

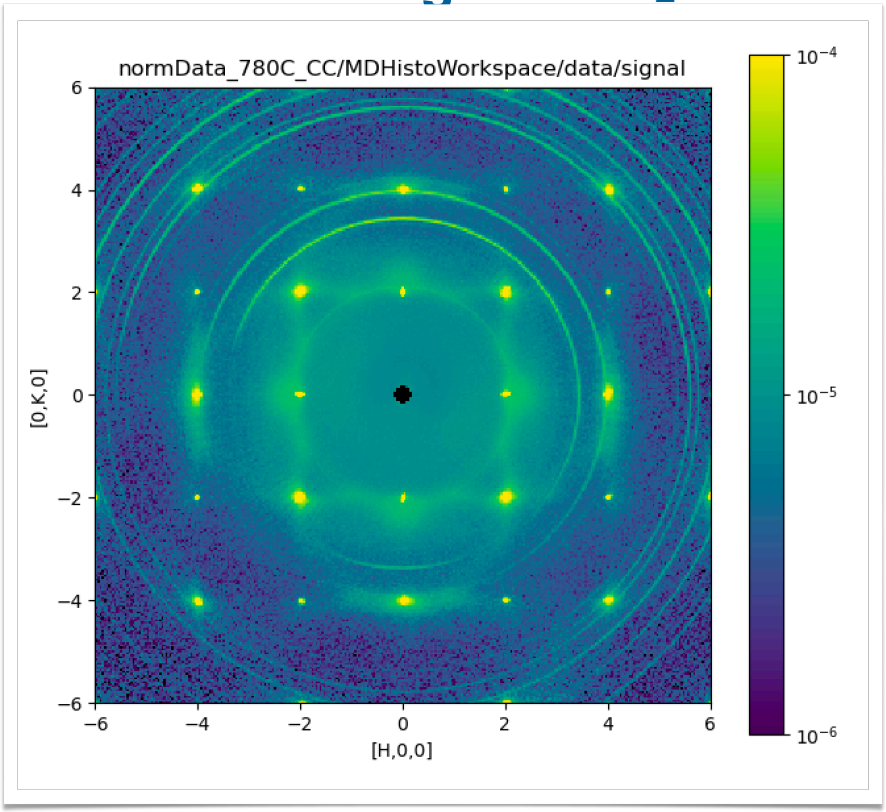

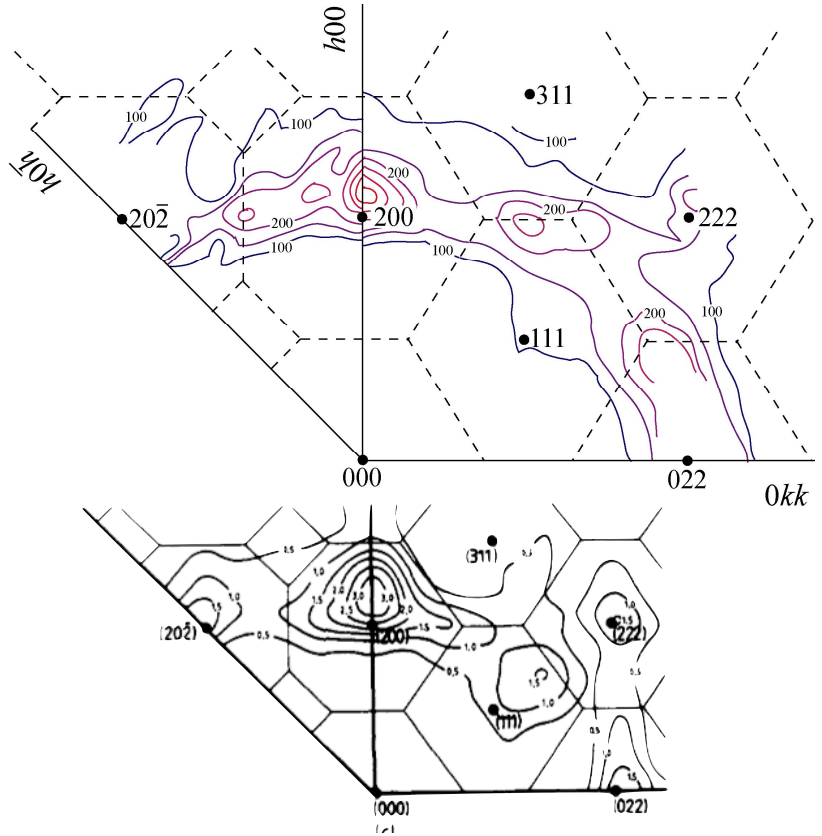

M. T. Hutchings *et al* J. Phys. C **17**, 3903 (1984)

RELAXOR FERROELECTRICS - $Pb(Mg_{1/3}Nb_{2/3})O_{3-x}PbTiO_3$

M. J. Krogstad, *et al*., Nat Mater **48**, 1 (2018).

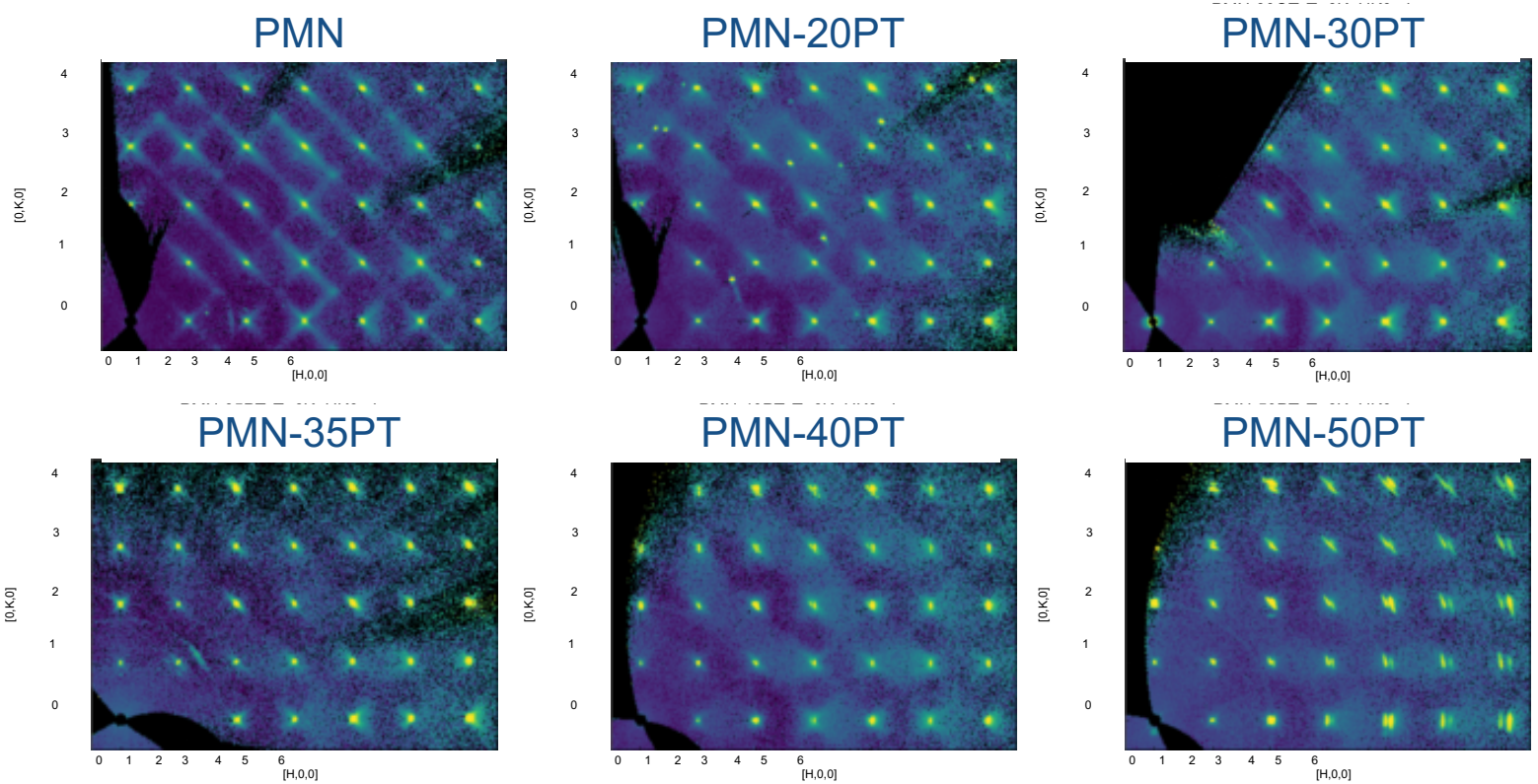

COMPLEMENTARITY OF NEUTRONS AND X-RAYS

$Pb(Mg_{1/3}Nb_{2/3})O_3$-30%$PbTiO_3$

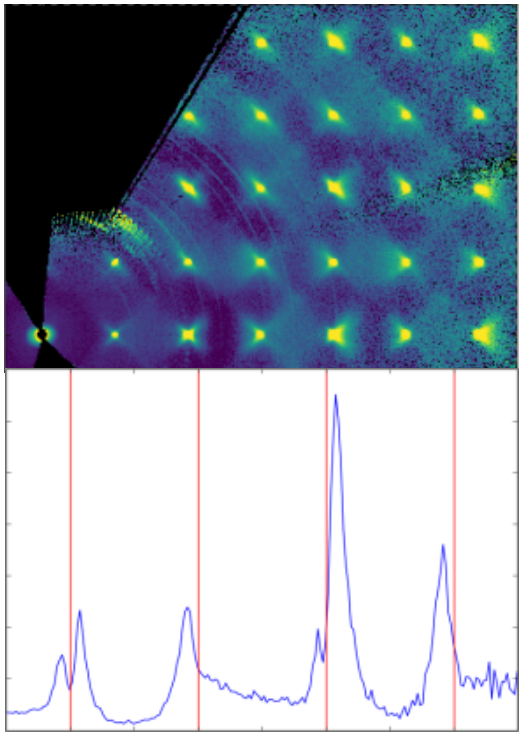

Corelli Neutrons

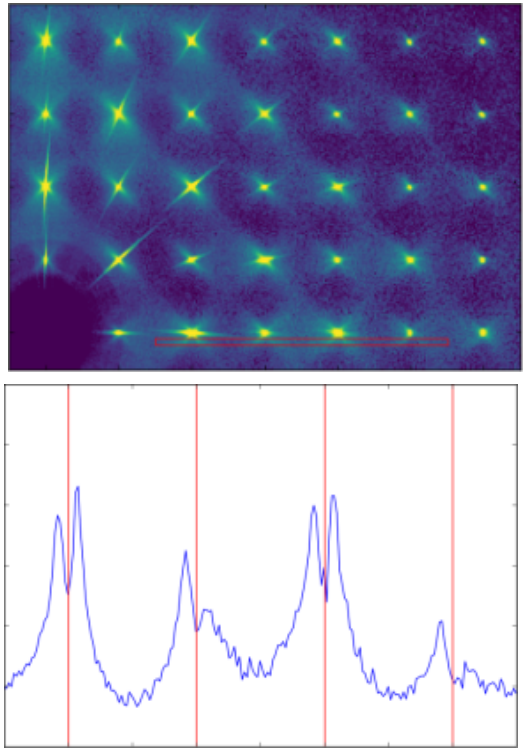

CHESS 55keV X-rays

THE FUTURE

- Advances in instrumentation have transformed our ability to measure single crystal total scattering over large volumes of reciprocal space.
  - High-Energy X-rays
  - Time-of-Flight Neutrons
- This is enabling new ways of analyzing the data:
  1. Unsupervised machine learning
  2. *ab initio* computational modeling
  3. 3D-ΔPDF - real-space pair distributions
- The results give unique insight into disordered materials
  - Bridging the gap between diffraction and imaging

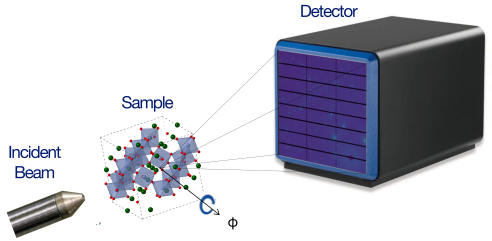

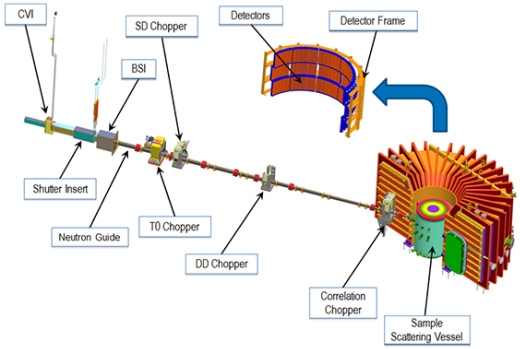

A FEW REFERENCES

- T. R. Welberry & B. Butler, Chem Rev **95**, 2369–2403 (1995).
- F. Frey, Acta Cryst B **51**, 592–603 (1995).
- T. R. Welberry & D. J. Goossens, Acta Cryst A **64**, 23–32 (2007).
- D. A. Keen & A. L. Goodwin, Nature News **521**, 303–309 (2015).